Triple-Pnictogen Bonding as a Tool for Supramolecular Assembly

Shiva Moaven,[a] Miranda C. Andrews,[a] Thomas J. Polaske,[b] Brian M. Karl,[b] Daniel K. Unruh,[a] Eric Bosch,[c] Nathan P. Bowling,[b] Anthony F. Cozzolino[a]**

Supplementary Information

a) Department of Chemistry and Biochemistry, Texas Tech University, 1204 Boston Avenue, Lubbock, TX 79409-1061, United States

b) Department of Chemistry, University of Wisconsin - Stevens Point, 2101 Fourth Avenue, Stevens Point, WI 54481, United States

c) Chemistry Department, Missouri State University, 901 S. National Ave., Springfield, MO 65897, United States

Table of Contents

S1 Experimental Details

S1.1 General Methods

The starting materials, antimony(III) chloride (99%, Strem Chemicals), diethylamine (+99%, Alfa Aesar), *n*-butyl lithium (2.5 M Hexane solution, Aldrich), 4,4-bipyridine (≥96%, CHEM-IMPEX INT'L INC.), tetrakis(triphenylphosphine)palladium(0) (99%, Strem Chemicals), copper iodide (98%, Strem Chemicals), 3-ethynylpyridine (98%, Sigma-Aldrich), tetrabutylammonium fluoride (1.0 M solution in THF, Sigma-Aldrich) and triethylamine (99%, Alfa Aesar) were used as purchased. Anhydrous benzene, and pyridine were prepared by heating and stirring over CaH_2 for 16 h, distilling under N_2 and storing over activated 3 Å molecular sieves inside a glovebox. Deuterated solvents, purchased from Cambridge Isotopes Laboratory, were degassed using three freeze-pump-thaw cycles before being transferred onto freshly activated molecular sieves. Tris(2-pyridylmethyl)amine (TPA) was prepared according to literature.[1] Air sensitive manipulations were performed in an N_2 purged inert atmosphere box (LC Technology Solutions Inc.). All NMR spectra were collected at 21-22 °C on a JEOL ECS 400 MHz NMR spectrometer. All IR spectra were obtained using a Nicolet iS 5 FT-IR spectrometer equipped with a Specac Di Quest ATR accessory. CHN analyses were obtained on-site with a Perkin Elmer 2400 Series II CHNS/O analyzer.

S1.2 Synthesis

S1.2.1 Preparation of 3,3'-((5-(tert-butyl)-2-((trimethylsilyl)ethynyl)-1,3-phenylene)bis(ethyne-2,1-diyl))dipyridine (**5**)

To a storage tube under Ar was added ((2,6-dibromo-4-(tert-butyl)phenyl)ethynyl)trimethylsilane[2] (2.00 g, 5.15 mmol), 3-ethynylpyridine (1.06 g, 10.27

mmol), and triethylamine (40 mL). Argon was bubbled through this mixture for 20 minutes before $Pd(PPh_3)_4$ (0.347 g, 0.300 mmol) and CuI (0.057 g, 0.300 mmol) were added. The tube was sealed under Ar and heated at 90 °C for 20 hours. After cooling to room temperature, the mixture was rinsed into a separatory funnel with CH_2Cl_2. The organic mixture was washed with water, dried with Na_2SO_4, filtered, and concentrated. Purification via flash chromatography (silica, 70% hexane:30% ethyl acetate) yielded the product off-white solid (1.428 g, 3.30 mmol, 64% yield). mp 106-113 °C. ^{1}H NMR (400 MHz, $CDCl_3$, δ ppm): 8.83 (dd, J = 2.1, 0.9 Hz, 2H), 8.58 (dd, J = 4.9, 1.7 Hz, 2H), 7.85 (dt, J = 7.9, 1.9 Hz, 2H), 7.56, (s, 2H) 7.31 (ddd, J = 7.9, 4.9, 0.9 Hz, 2H), 1.35 (s, 9H), 0.28 (s, 9H) ppm. ^{13}C{^{1}H} NMR (100 MHz, $CDCl_3$, δ ppm):152.3, 151.4, 148.7, 138.3, 129.1, 125.5, 125.3, 122.9, 120.2, 103.0, 101.6, 91.4, 89.5, 34.7, 30.8, 0.0. FTIR(Di-ATR, cm^{-1}) 3028 (w, Csp^2–H), 2955 (m, Csp^3–H), 2151 (m, $C_{sp}{\equiv}C_{sp}$). HRMS (ESI) *m/z* $[M+H]^+$ calculated for $C_{29}H_{29}N_2Si$ 433.2100 found 433.2098.

S1.2.2 Preparation of 3,3'-((5-(tert-butyl)-2-ethynyl-1,3-phenylene)bis(ethyne-2,1-diyl))dipyridine (**4**)

Compound **5** (2.69 g, 6.22 mmol) was dissolved in THF (30 mL) under an Ar atmosphere. The flask was chilled to −89 °C (liq. N_2 /2-propanol) before TBAF (6.22 mL, 1M solution in THF, 6.22 mmol) was added. The mixture was stirred at this temperature for 20 min under Ar before NH_4Cl solution was added. This mixture was extracted with EtOAc. The organic layer was separated, dried with $MgSO_4$, filtered, and concentrated. The product was loaded onto a flash column (silica) with 100% EtOAc. Polarity was gradually increased via addition of small portions of methanol. Appropriate fractions were concentrated to reveal the product as an off-white powder (1.75, 4.86 mmol, 78% yield).). mp 137-145 °C. ^{1}H NMR (400 MHz, $CDCl_3$, δ ppm): 8.84 (dd, J = 2.2, 0.9 Hz, 2H), 8.57 (dd, J = 4.9, 1.7 Hz, 2H), 7.86 (dt, J = 7.9, 1.9 Hz, 2H), 7.59 (s, 2H), 7.29 (ddd, J =

7.9, 4.9, 0.9 Hz, 2H), 3.68 (s, 1H), 1.35 (s, 9H). $^{13}C\{^{1}H\}$ NMR (100 MHz, $CDCl_3$, δ ppm): 152.4, 151.8, 148.8, 138.5, 129.3, 125.9, 124.3, 123.0, 120.2, 91.1, 89.8, 85.1, 80.6, 34.8, 30.9. FTIR (Di-ATR, cm^{-1}) 3150 (s, C_{sp}–H), 2959(s, Csp^3–H), 2092(m, $C_{sp}\equiv C_{sp}$). HRMS (ESI) *m/z* $[M+H]^+$ calculated for $C_{26}H_{21}N_2$ 361.1705 found 361.1713.

S1.2.3 Preparation of 1,3,5-tris((4-(tert-butyl)-2,6-bis(pyridin-3-ylethynyl)phenyl)ethynyl)benzene (**3**)

To a storage tube under Ar was added compound **4** (0.201 g, 0.56 mmol) and 1,3,5-triiodobenzene (0.084 g, 0.18 mmol), and triethylamine (20 mL). THF was added (5 mL) and Argon was bubbled through this mixture for 20 minutes before $Pd(PPh_3)_4$ (0.064 g, 0.055 mmol) and CuI (0.011 g, 0.058 mmol) were added. The tube was sealed under Ar and heated at 80 °C for 20 hours. After cooling to room temperature, a precipitate was observed and two crops were collected by filtration. The first crop contained protonated triethylamine and was discarded. The second crop and filtrate were rinsed into a separatory funnel with CH_2Cl_2. The organic mixture was washed with 5% NaOH solution, dried with $MgSO_4$, and concentrated. The product was loaded onto a flash column (silica) with 100% EtOAc. Polarity was gradually increased via addition of small portions of methanol. Appropriate fractions were concentrated to reveal the product as a light brown/white solid (0.159 g, 0.138 mmol, 77% yield). mp 182-184 °C. ^{1}H NMR (400 MHz, $CDCl_3$, δ ppm): 8.70 (s, 6H), 8.41 (s, 6H), 7.75 (m, 9H), 7.63 (s, 6H), 1.41 (s, 27H). $^{13}C\{^{1}H\}$ NMR (100 MHz, $CDCl_3$, δ ppm): 152.02, 151.99, 148.8, 138.5, 134.1, 129.5, 125.5, 124.7, 124.6, 123.2, 120.0, 95.2, 91.3, 90.1, 88.8, 35.0, 31.0. FTIR (Di-ATR, cm^{-1}) 3025 (w, Csp^2–H), 2951 (w, Csp^3–H). HRMS (ESI) *m/z* $[M+H]^+$ calculated for $C_{84}H_{61}N_6$ 1153.4958 found 1153.4951.

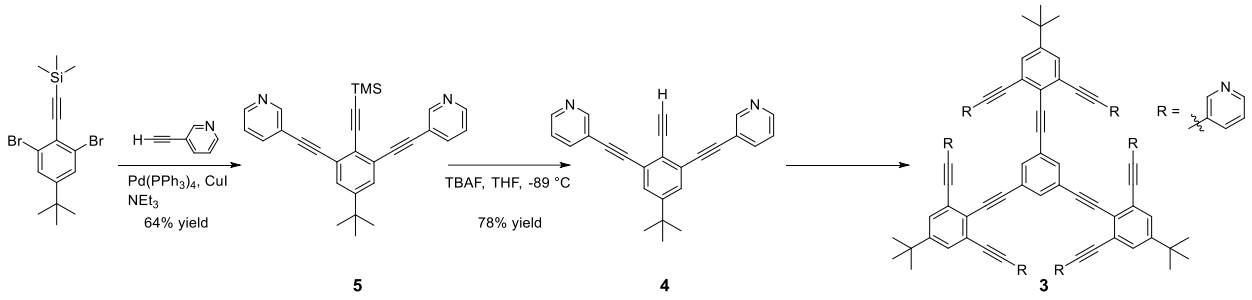

Scheme S1. Synthesis of **3**.

S1.2.4 Preparation of antimony(III) diethylamide, $Sb(NEt_2)_3$

The following is a modification of a literature procedure.[3] All manipulations were performed under a nitrogen atmosphere. Lithium diethylamide (4.75 g, 60.0 mmol) was suspended in 60 mL of THF and cooled down to −70 °C. Antimony(III) chloride (4.52 g, 19.8 mmol) was dissolved in 40 mL of cold THF (−35 °C) and slowly added to the lithium diethylamide suspension while stirring. After the addition of antimony(III) chloride was complete, the mixture was allowed to warm up to room temperature and was stirred for 18 hours in the dark. The solvent was removed under vacuum and the residue was dissolved in 100 mL of hexanes and filtered through a bed of Celite. The yellow solution was taken to dryness under reduced pressure yielding an orange-yellow liquid. Yield 4.97 g (74.2%, 14.7 mmol). ^{1}H NMR (400 MHz, C_6D_6, δ ppm): 1.09 (t, J=7.10 Hz, 18H, $Sb(N(CH_2C\mathit{H}_3)_2)_3$), 3.17 (q, J=7.02 Hz, 12H, $Sb(N(C\mathit{H}_2CH_3)_2)_3$). $^{13}C\{^1H\}$ NMR (100.6 MHz, C_6D_6, δ ppm): 16.63 ($Sb(N(CH_2\underline{C}H_3)_2)_3$), 42.23 ($Sb(N(\underline{C}H_2CH_3)_2)_3$). FTIR (Di-ATR, cm^{-1}) 2959 (vs, Csp^3–H), 1177 (s, C–N), 567 (m, Sb–N).

S1.2.5 Preparation of 2,2',2"-triskatyl methane, $(C_9H_8N)_3CH$ (**1**)

The synthesis was based on previously reported method.[4] 3-Methylindole (3.93 g, 29.9 mmol) was suspended in 5 mL of methanol. Triethyl orthoformate (1.7 mL, 10 mmol) was added to the solution and the solution was warmed to 50 °C. Three drops of sulfuric acid were added to the solution which resulted in a color change from brown to purple and eventually precipitation of the product. The reaction mixture was allowed to cool to room temperature before the precipitate was

recovered by filtration. Rinsing with methanol gave a green-gray solid. Yield 3.10 g (7.68 mmol, 77.1%), mp 315-318 °C. ^{1}H NMR (400 MHz, $CDCl_3$, δ ppm): 2.20 (s, 9H), 6.24 (s, 1H), 7.19 (m, 6H), 7.26 (d, *J*=7.8, 3H), 7.6 (d, *J*=6.9 Hz, 3H), 7.72 (s, 3H). FTIR (Di-ATR, cm^{-1}) 3400 (s, N–H), 3051 (w, Csp^2–H), 2925(w, Csp^3–H).

S1.2.6 Synthesis of **2**

Compound **1** (1.21 g, 3.00 mmol) was suspended in 30 mL of anhydrous benzene. A benzene solution of antimony(III) diethylamide (1.05 g, 3.10 mmol) was added slowly to the green-gray suspension and the solution turned cloudy and dark yellow in color. After the addition was complete, the solvent was removed under reduced pressure. The faint yellow solid was suspended in anhydrous hexanes, filtered and dried to give an analytically pure material with half of a molecule of benzene per **2** based on ^{1}H NMR and elemental analysis. Yield 1.58 g (2.81 mmol, 93.7%). mp 198-202 °C (dec.). ^{1}H NMR ($CDCl_3$, δ ppm): 2.46 (s, 9H), 6.16 (s, 1H), 7.08 (t, *J*=6.84, 3H), 7.16 (t, *J*=6.84, 3H), 7.45 (m, 6H). $^{13}C\{^{1}H\}$ NMR ($CDCl_3$, δ ppm): 8.82, 33.10, 108.16, 111.43, 119.30, 120.16, 121.93, 128.49, 130.95, 136.30, 139.81. FTIR (ATR, cm^{-1}) 3040 (w, Csp^2–H), 2913 (w, Csp^3–H). Anal. Calc. for $C_{31}H_{25}SbN_3$: C, 66.33; H, 4.49.N, 7.49. Found: C, 66.66; H, 4.53, N, 6.98).

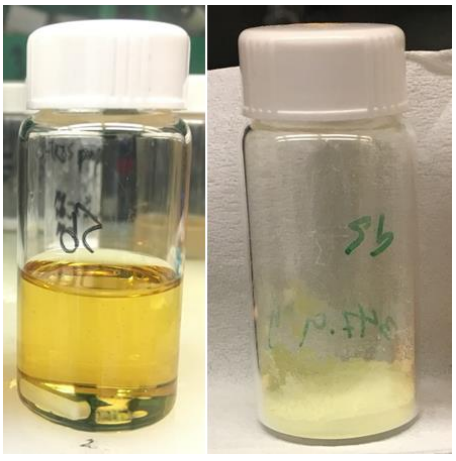

Figure S1. Preparation of **2**. Left: after addition of $Sb(NEt_2)_3$ to **1** and right: dried **2** powder.

S1.2.7 Preparation of **2**·Py_2

In a 20 mL vial, 54 mg (0.096 mmol) of **2**·½C_6H_6 was partially dissolved in 2 mL of anhydrous benzene. An excess of pyridine (0.5 mL) was added to the mixture. Upon the addition of the pyridine, the mixture became colorless and homogeneous. After 24 hours colorless block-shaped crystals, suitable for single crystal X-ray diffraction were recovered from the solution. Yield 34 mg (0.038 mmol 40%). mp 203 °C (dec.), phase change observed at 190 °C. ^{1}H NMR ($CDCl_3$, δ ppm): 2.48 (s, 9H), 6.18 (s, 1H), 6.93 (m, 6H), 7.21 (m, 6H), 7.41 (d, *J*=6.88 Hz, 4H), 7.66 (d, *J*=7.32 Hz, 4H), 8.46 (d, *J*=5.96 Hz, 4H). ^{13}C{^{1}H} NMR ($CDCl_3$, δ ppm): 8.86, 29.87, 107.50, 111.27, 119.15, 119.65, 121.45, 124.18, 128.50, 130.95, 136.77, 137.19, 139.84, 149.18. FTIR (ATR, cm^{-1}) 3048 (w, Csp^2–H), 2920 (m, Csp^3–H).

S1.2.8 Preparation of **2**·BP

In a 20 mL vial, 54 mg (0.096 mmol) of **2**·½C_6H_6 and 23 mg (1.47 mmol) of 4,4'-bipyridine were dissolved in 5 mL of anhydrous toluene. Upon the addition of toluene, the mixture became yellow and homogeneous. Upon sitting at ~20 °C for 24 hours blade-shaped yellow crystals, suitable for single crystal X-ray diffraction, were recovered from the solution. PXRD confirmed phase purity (see Fig. S36). Yield 46 mg (0.053 mmol, 55%). mp 200 °C (dec). ^{1}H NMR ($CDCl_3$, δ ppm): 2.52 (s, 9H), 6.22 (s, 1H), 6.90 (t, $J_=$8.24 Hz, 3H), 6.96 (t, $J_=$6.88 Hz, 3H), 7.09 (d, *J*=7.80 Hz, 3H), 7.30 (d, *J*=6.40 Hz, 4H), 7.43 (d, *J*=7.80 Hz, 3H), 8.41 (d, *J*=5.96 Hz, 4H). ^{13}C{^{1}H} NMR ($CDCl_3$, δ ppm): 8.89, 33.23, 107.09, 111.14, 119.06, 119.32, 121.10, 121.87, 130.95, 137.77, 139.82, 145.97, 149.60. FTIR (Di-ATR, cm^{-1}) 3024 (m, Csp^2–H), 2895 (w, Csp^3–H). Anal. Calc. for $C_{52}H_{46}N_5Sb$: C, 72.39; H, 5.37; N, 8.12. Found: C, 72.80; H, 5.11; N, 8.05).

S1.2.9 Preparation of **2**·TPA

In a 20 mL vial, 54 mg (0.096 mmol) of **2**·½C_6H_6 and 29 mg of TPA (0.099 mmol) were dissolved in 2 mL of anhydrous toluene where it formed an orange homogeneous solution. Upon sitting at ~20 °C for 24 hours needle-shaped colorless crystals, suitable for single crystal X-ray diffraction, were recovered from the solution. PXRD confirmed phase purity (see Fig. S37). Yield 71 mg (0.078 mmol, 81%). mp 195 °C (dec.), phase change observed at 175-185 °C. ^{1}H NMR ($CDCl_3$, δ ppm): 2.54 (s, 9H), 4.15 (s, 6H), 6.27 (s, 1H), 6.64 (t, J=7.32 Hz, 3H), 6.87 (m, 9H), 7.37 (d, J=6.52 Hz, 3H), 7.42 (d, J=7.76 Hz, 3H), 7.61 (t, J=7.80 Hz, 3H), 7.93 (d, J=4.60 Hz, 3H). ^{13}C{^{1}H} NMR ($CDCl_3$, δ ppm): 8.99, 33.62, 57.17, 105.88, 111.72, 118.39, 118.47, 120.02, 122.97, 124.23, 130.92, 137.04, 139.19, 140.30, 149.51, 157.32. FTIR (Di-ATR, cm^{-1}) 3040 (m, Csp^2–H), 2913 (m, Csp^3–H). Anal. Calc. for $C_{53}H_{48}N_7Sb$: C, 70.36; H, 5.35; N, 10.84. Found: C, 70.31; H, 5.25; N, 10.89).

S1.2.10 Preparation of **2**$_2$·**3**

In 4 mL shell vial, 3.3 mg (0.0033 mmol) of **3** and 3.3 mg (0.0033 mmol) of **2**·½C_6H_6 were dissolved in 0.5 mL of anhydrous benzene and gently heated until all solids were dissolved in the solution. Upon sitting at ~20 °C for 24 hours colorless block-shaped colorless crystals were recovered from the solution. The recovered crystals appeared to be two different crystals habits (α and β) and they were both suitable for single crystal X-ray diffraction. Yield 51% (5.9 mg, based on $C_{230}H_{194}N_{12}Sb_2$). FTIR (Di-ATR, cm^{-1}) 3031 (m, Csp^2–H), 2956, 2860 (m, Csp^3–H).

S1.3 Crystallography

Single crystal data was collected for **2**, **2**·2Py, **2**·BP, **2**·TPA, α-$\mathbf{2}_2$·**3**, and β-$\mathbf{2}_2$·**3** on a Bruker PLATFORM three circle diffractometer equipped with an APEX II CCD detector and operated at 1500 W (50kV, 30 mA) for **2** and 1350 W (40kV, 30 mA) for **2**·2Py, **2**·BP, , **2**·TPA, α-$\mathbf{2}_2$·**3**, and β-$\mathbf{2}_2$·**3** to generate (graphite monochromated) Mo Kα radiation (λ = 0.71073 Å). Crystals were transferred from the vial and placed on a glass slide in polyisobutylene. A Zeiss Stemi 305 microscope was used to identify a suitable specimen for X-ray diffraction from a representative sample of the material. The crystal and a small amount of the oil were collected on a MīTiGen cryoloop and transferred to the instrument where it was placed under a cold nitrogen stream (Oxford) maintained at 100 K throughout the duration of the experiment. The sample was optically centered with the aid of a video camera to ensure that no translations were observed as the crystal was rotated through all positions.

A unit cell collection was carried out followed by the collection of a sphere of data. Omega scans were carried out with a 90, 60, 20, 30, 60, and 15 sec/frame exposure time for **2**, **2**·2Py, , **2**·BP, **2**·TPA, α-$\mathbf{2}_2$·**3**, and β-$\mathbf{2}_2$·**3** respectively, and a rotation of 0.50° per frame for all samples. After data collection, the crystals were measured for size, morphology, and color. The values are reported in Table S1.

Intensity data were corrected for Lorentz, polarization, and background effects using the Bruker program APEX 3.[5] A semi-empirical correction for adsorption was applied using the program *SADABS*.[6] The *SHELXL-2014* series of programs were used for the solution and refinement of the crystal structure.[7] Hydrogen atoms bound to carbon atoms were located in the difference Fourier map and were geometrically constrained using the appropriate AFIX commands. The RIGU restraint was used globally for each structure.

S1.4 Powder X-ray Diffraction

The diffraction patterns for **2**, **2**·Py_2, **2**·BP, **2**·TPA were collected on a Rigaku Ultima III powder diffractometer. X-ray diffraction patterns were obtained by using a 2θ scan with the source fixed at 0° and the detector scanning a θ range of 3-60°, step size of 0.02°, and scan time of 10 min/degree. The X-ray source was Cu Kα radiation (λ=1.5418 Å) with an anode voltage of 40 kV and a current of 44 mA. The beam was then discriminated by Rigaku's Cross Beam parallel beam optics to create a monochromatic parallel beam. Diffraction intensities were recorded on a scintillation detector after being filtered through a Ge monochromator.

Samples of **2**, **2**·Py_2, **2**·BP, **2**·TPA were packed inside borosilicate capillaries with inner diameter of 0.7 mm and wall thickness of 0.01 mm purchased from Charles Supper Company. Samples were prepared under inert atmosphere and the tubes were sealed with grease. After sealing they were mounted on a capillary holder and data was collected. The resulting diffractograms were processed with the software JADE v9.1. Simulated patterns were obtained from single crystal data of each sample using the Mercury 3.10 software and the appropriate X-ray wavelength.

Table S1. Crystal data and structure refinement for **2**, **2**·Py_2, **2**·BP, **2**·TPA, α-$\mathbf{2}_2$·**3,** β-$\mathbf{2}_2$·**3**.

	2	**2**·Py_2	**2**·BP	**2**·TPA	α-$\mathbf{2}_2$·**3**	β-$\mathbf{2}_2$·**3**
Crystal Color	yellow	colorless	yellow	colorless	colorless	colorless
Crystal Habit	block	plate	blade	needle	block	block
Empirical formula	$C_{34}H_{28}N_3Sb$	$C_{44}H_{38}N_5Sb$	$C_{52}H_{46}N_5Sb$	$C_{53}H_{48}N_7Sb$	$C_{230}H_{194}N_{12}Sb_2$	$C_{245}H_{209}N_{12}Sb_2$
Formula weight	600.37	758.56	862.69	904.73	3369.46	3564.73
Temperature [K]	100(2)	100(2)	100(2)	200(2)	100(2)	100(2)
Wavelength [Å]	0.71073	0.71073	0.71073	0.71073	0.71073	0.71073
Crystal system	Trigonal	Tetragonal	Monoclinic	Triclinic	Triclinic	Triclinic
Space group	$R\bar{3}$	$P\bar{4}2_1m$	$P2_1/c$	$P\bar{1}$	$P\bar{1}$	$P\bar{1}$
Unit cell dimensions [Å]	*a* = 13.969(3) α=90 ° *b* = 13.969(3) β=90 ° *c* = 23.297(5) γ=120°	*a* = 17.4727(16) α=90 ° *b* = 17.4727(16) β=90 ° *c* = 13.1393(12) γ=90°	*a* = 14.2491(17) α=90 ° *b* = 13.1684(16) β=90.8890(10) ° *c* = 22.046(3) γ=90°	*a* = 10.7750(12) α=77.5670(10) ° *b* = 13.1908(14) β=78.598(2) ° *c* = 17.3921(19) γ=66.3250(10)°	*a* = 21.039(10) α=71.889(8) ° *b* = 21.293(10) β=67.825(10) ° *c* = 23.832(10) γ=85.397(10)°	*a* = 15.0609(19) α=78.624(2) ° *b* = 25.978(3) β=81.029(2) ° *c* = 26.390(3) γ=84.937(2)°
Volume [$Å^3$]	3936.9(18)	4011.4(8)	4136.2(9)	2193.7(4)	9389(7)	9981(2)
Z	6	4	4	2	2	2
Calculated density [g/cm^3]	1.519	1.256	1.385	1.370	1.192	1.186
Absorption coefficient [mm^{-1}]	1.080	0.723	0.710	0.674	0.346	0.329
F(000)	1824	1552	1776	932	3520	3730
Crystal size [mm]	0.090 × 0.085 × 0.035	0.285 × 0.240 × 0.060	0.480 × 0.470 × 0.095	0.480 × 0.065 × 0.055	0.380 × 0.185 × 0.115	0.480 × 0.470 × 0.455
Theta range for data collection	1.897 to 25.440°	2.263 to 25.371°	1.429 to 27.135°	1.208 to 27.293°	1.007 to 25.479°	1.484 to 27.230°
Limiting indices	$-16\le h\le 16$ $-16\le k\le 16$ $-28\le l\le 28$	$-21\le h\le 21$ $-21\le k\le 21$ $-15\le l\le 15$	$-18\le h\le 18$ $-16\le k\le 16$ $-28\le l\le 28$	$-13\le h\le 13$ $-17\le k\le 16$ $-22\le l\le 22$	$-25\le h\le 23$ $-25\le k\le 25$ $-28\le l\le 28$	$-19\le h\le 19$ $-33\le k\le 33$ $-33\le l\le 33$

	2	**2**·Py_2	**2**·BP	**2**·TPA	α-$\mathbf{2}_2$·**3**	β-$\mathbf{2}_2$·**3**
Reflections collected / unique	13317/1630 [R(int) = 0.0527]	40896/3860 [R(int) = 0.0495]	47210/9133 [R(int) = 0.0403]	39104/9806 [R(int) = 0.0499]	150220/34577 [R(int) = 0.0879]	155884/44322 [R(int) = 0.0555]
Completeness to theta = 25.242°	100.0%	100.0%	100.0%	100.0%	99.9%	99.8%
Refinement method	Full-matrix least-squares on F^2	Full-matrix least-squares on F^2	Full-matrix least-squares on F^2	Full-matrix least-squares on F^2	Full-matrix least-squares on F^2	Full-matrix least-squares on F^2
Data / restraints / parameters	1630/105/121	3860/718/346	9133/0/528	9806/513/554	34577/2466/2425	44322/2746/2479
Goodness-of-fit on F^2	1.147	1.027	1.032	1.021	1.022	1.149
Final R indices [I>2sigma(I)]	R1 = 0.0296, wR2 = 0.0618	R1 = 0.0344, wR2 = 0.0773	R1 = 0.0265, wR2 = 0.0614	R1 = 0.0353, wR2 = 0.0677	R1 = 0.0604, wR2 = 0.1274	R1 = 0.0773, wR2 = 0.1644
R indices (all data)	R1 = 0.0349, wR2 = 0.0632	R1 = 0.0486, wR2 = 0.0830	R1 = 0.0331, wR2 = 0.0647	R1 = 0.0510, wR2 = 0.0730	R1 = 0.1235, wR2 = 0.1521	R1 = 0.1041, wR2 = 0.1740
Largest diff. peak and hole [$e \cdot A^{-3}$]	0.746 and −1.078	0.466 and −0.229	0.452 and −0.321	0.434 and −0.653	0.731 and −0.797	1.214 and −1.591

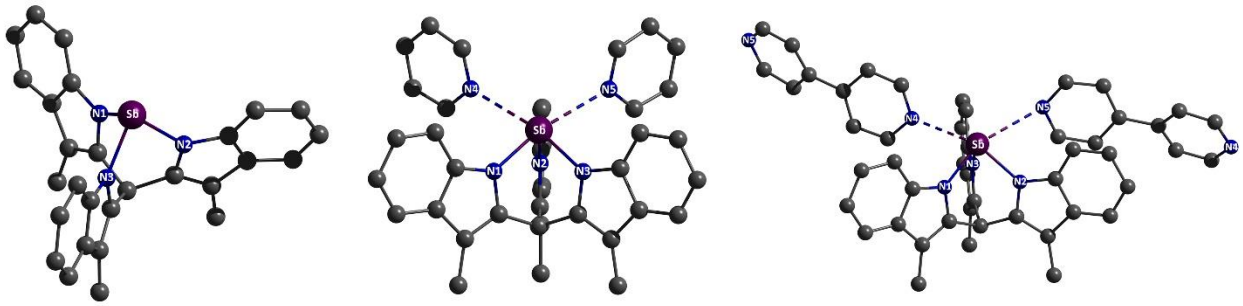

Figure S2. Left to right: Ball and stick representation of **2**, **2**·Py_2, and **2**·BP (hydrogens are omitted for clarity).

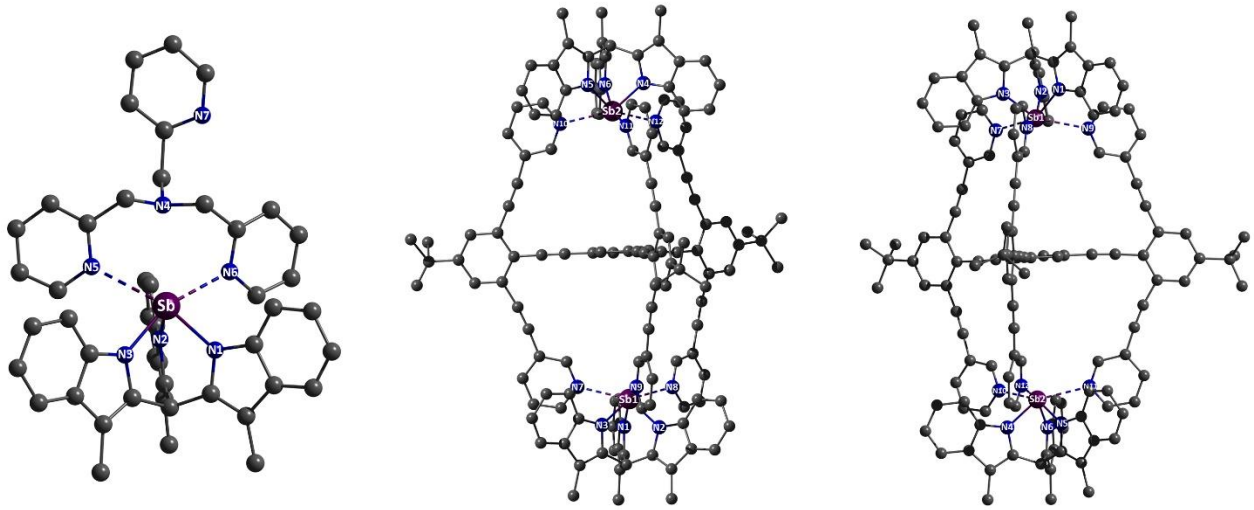

Figure S3. Left to right: Ball and stick representation of **2**·TPA, α-$\mathbf{2}_2$·**3**, and β-$\mathbf{2}_2$·**3** (hydrogens and solvent molecules are omitted for clarity).

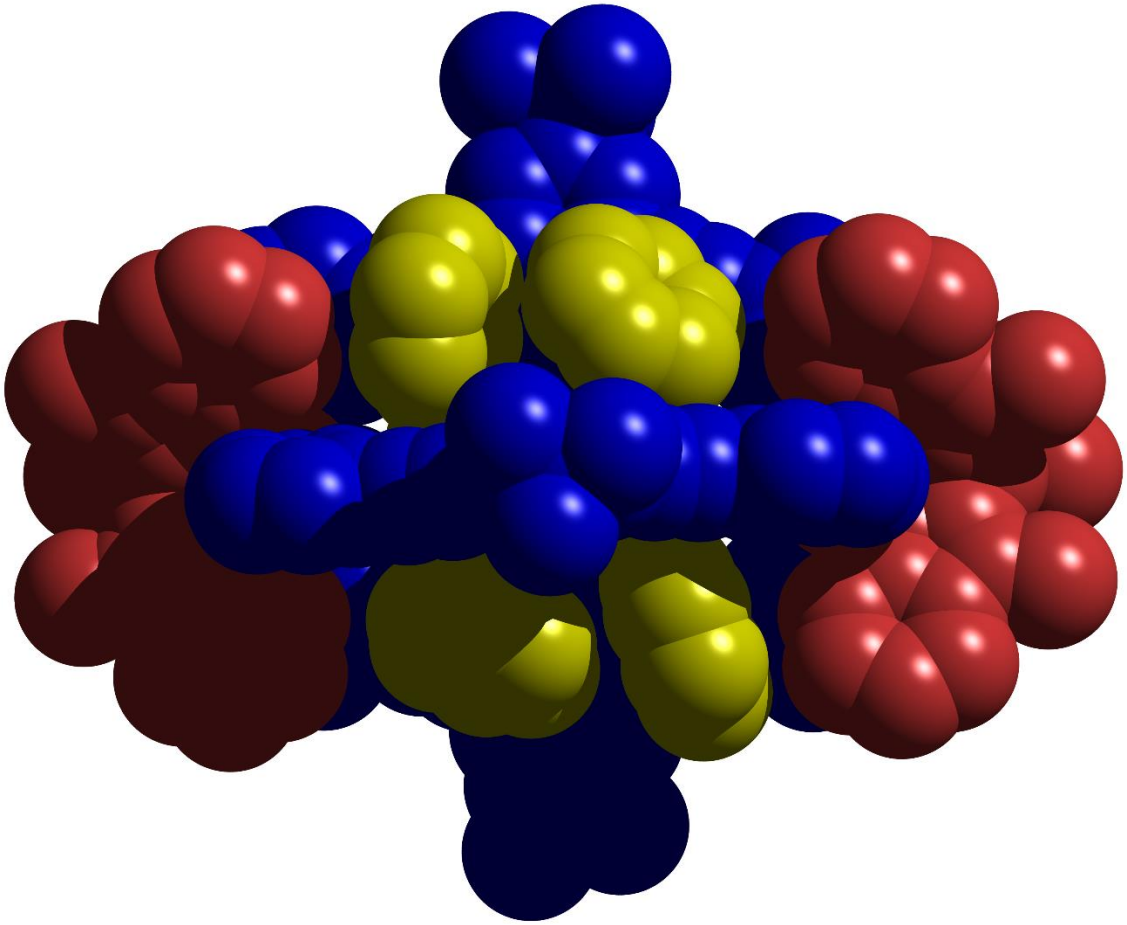

Figure S4. Space-filling (without hydrogen atoms) model of β-$\mathbf{2}_2$·**3** and solvent molecules surrounding the cavity windows. Each component is represented in a single color: **2**, **3**, and benzene molecules are in red, blue, and yellow, respectively.

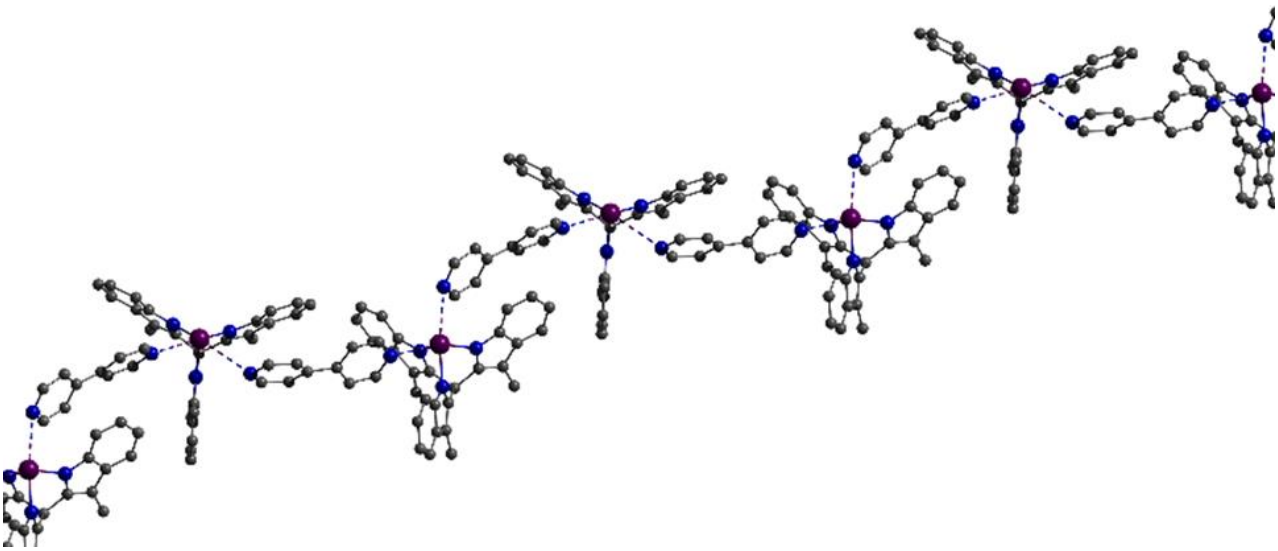

Figure S5. Formation of 1-D chain of **2**·BP in solid state. Sb: purple, N: blue, and C: gray. (hydrogens are omitted for clarity).

S1.5 Computational Methods

Calculations were performed using the ORCA 4.0 quantum chemistry program package from the development team at the Max Planck Institute for Bioinorganic Chemistry.[8] The starting geometry for optimization of **2** was based on the solved crystal structure of **2**. All calculations were carried out using the Zero-Order Regular Approximation (ZORA).[9,10] For geometry optimizations, frequencies, and thermochemistry the B97-D3[11] functional and def2-TZVPP[12,13] with SARC/J basis sets[14] were used for hydrogen atoms and all other atoms respectively. Spin-restricted Kohn–Sham determinants[15] were chosen to describe the closed shell wavefunctions, employing the RI approximation[16] and the tight SCF convergence criteria provided by ORCA. The basis set superposition error (BSSE) was corrected using the Boys and Bernardi procedures.[17] Molecular electrostatic potential (ESP) mapping was performed on the 0.001 isosurface of the electron density using the Multiwfn program. [18,19] All visualizations of ESP maps were performed with the Gabedit graphical interface software.[20] The cartesian coordinates of the geometry optimized molecules and supramolecules are provided as .xyz files in a .zip file.

Table S2. Energetics for gas phase monomers, dimers, trimer, and tetramer.

	E(Eh)	ZPE (Eh)	BSSE (kJ/mol)
2	-7820.421456	0.42226583	
2·Py	-8068.841129	0.51195405	3.667
2·Py_2	-8317.25803	0.60115615	6.541
2·Py_3	-8565.671124	0.6899784	8.812
Py	-248.3897371	0.08797053	
2·TPA[a]	-8736.61912		
2·TPA[b]	-8736.616104		
TPA	-916.1291653		

a) Conformation with 4 points of attachment (see Figure S6)

b) Conformation with 3 points of attachment as observed in the crystal structure (see Figure S6)

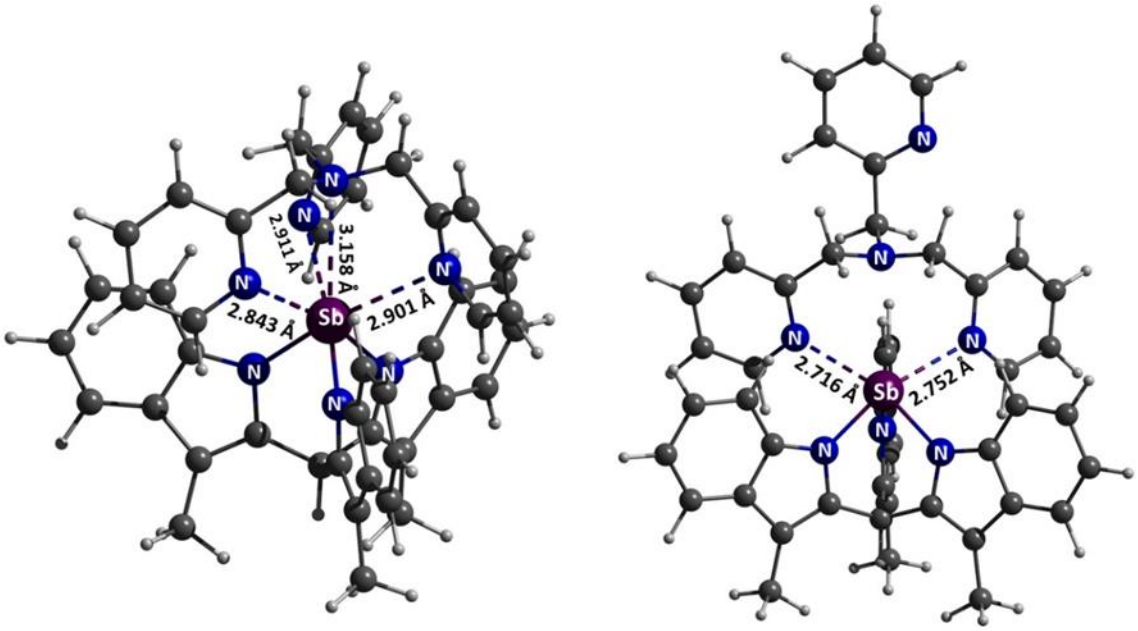

Figure S6. Geometry optimized structures of **2**·TPA[a] (left), and **2**·TPA[b] (right).

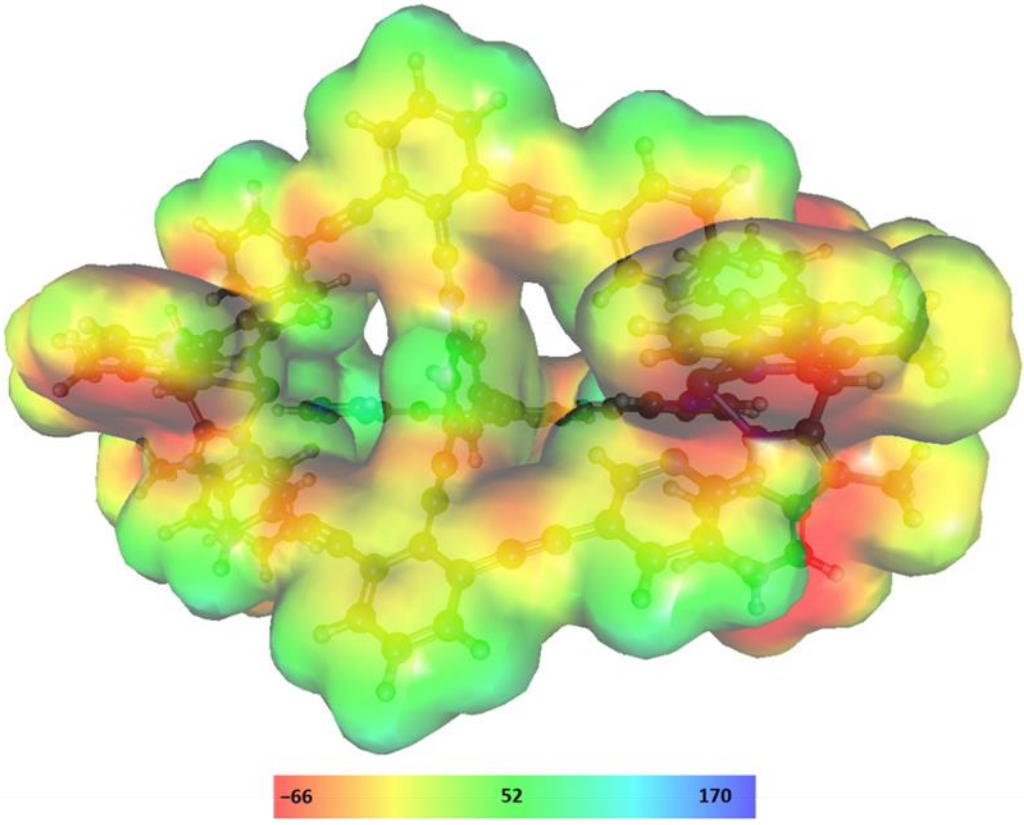

Figure S7. ESP map of $\mathbf{2}_2$·**3** supramolecule (*tert*-butyl groups were replaced by H atoms to speed up the amount of the computation time). ESP units are in kJ/mol.

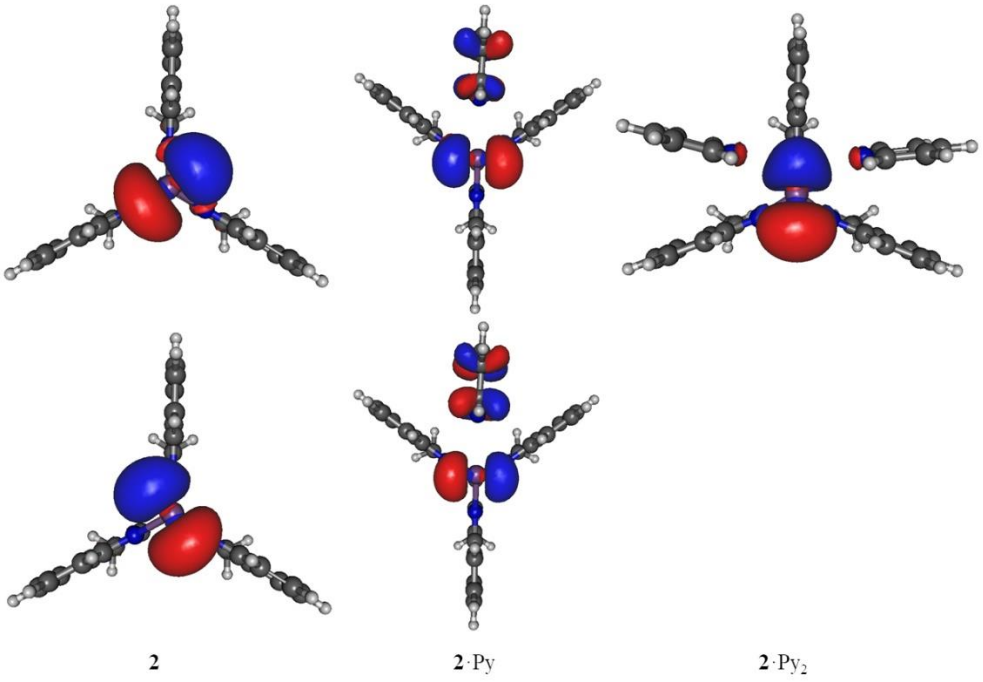

Figure S8. Low-energy unoccupied orbitals with Sb–N σ* orbitals of **2** (LUMO+1, and LUMO), **2**·Py (LUMO+2, and LUMO+1) and **2**·Py_2 (LUMO+4) top to bottom.

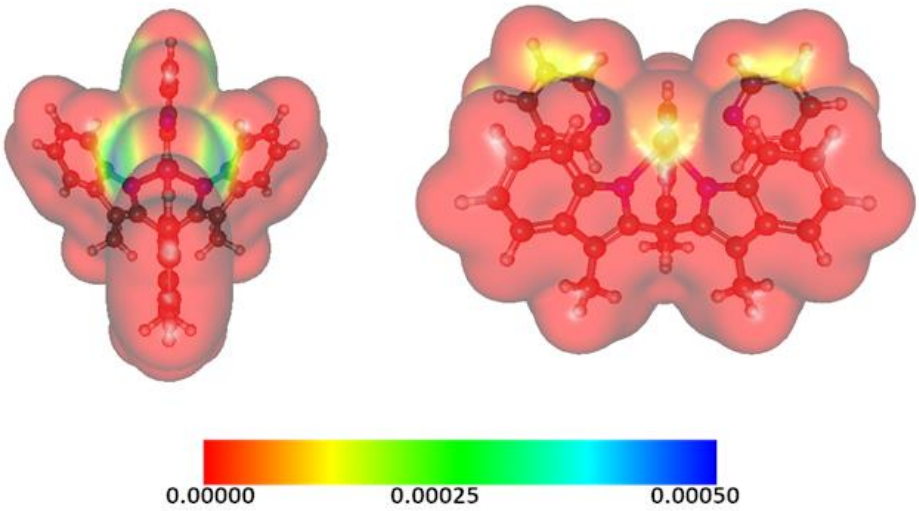

Figure S9. Fukui function integrated from above of **2**·Py (left) and **2**·Py_2 (right) mapped on the electron density surface (0.001 au isosurface).

S2 Spectroscopic Data

S2.1 ^{1}H NMR

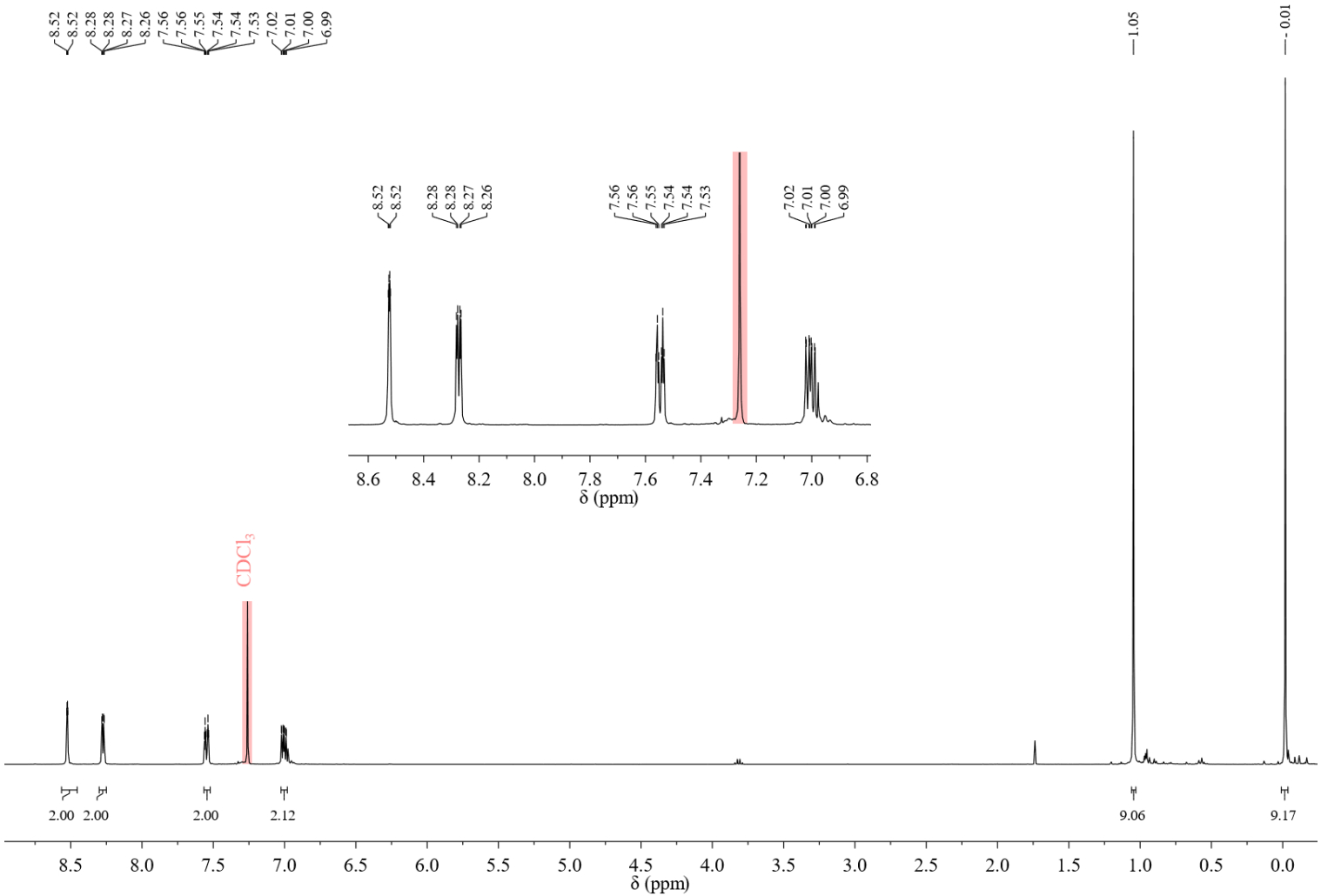

Figure S10. ^{1}H NMR of **5** in $CDCl_3$.

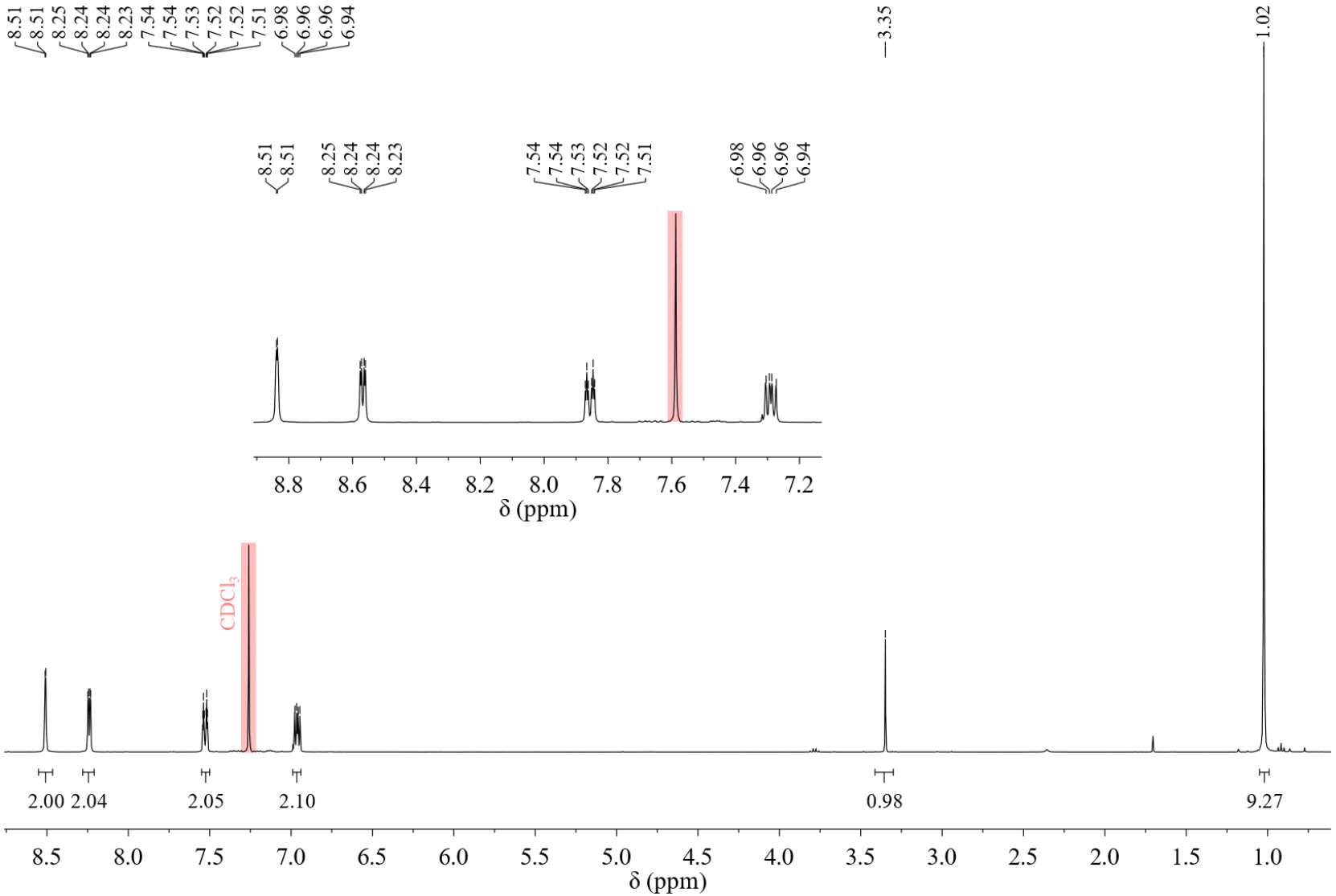

Figure S11. ^{1}H NMR of **4** in $CDCl_3$.

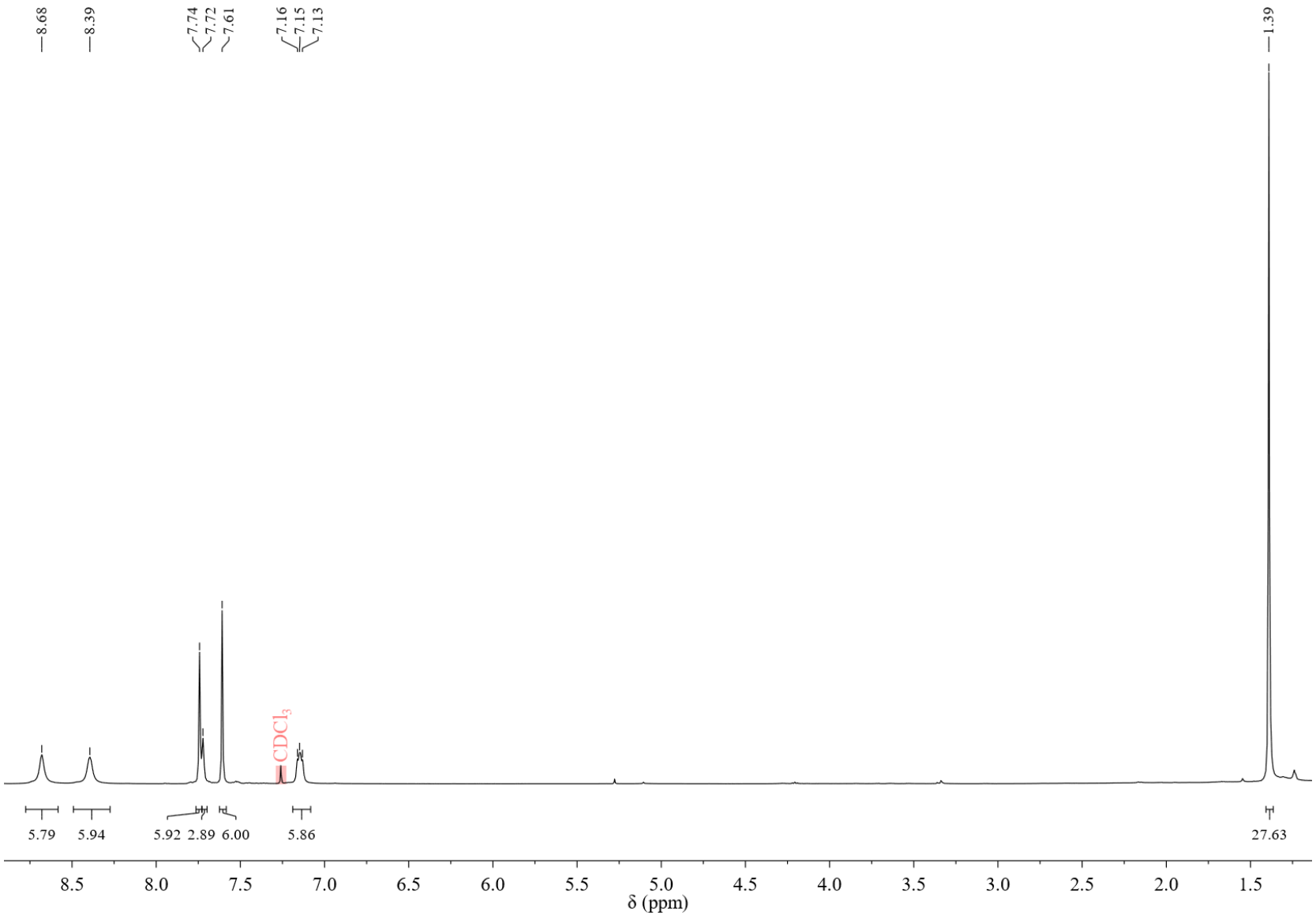

Figure S12. ^{1}H NMR of **3** in $CDCl_3$.

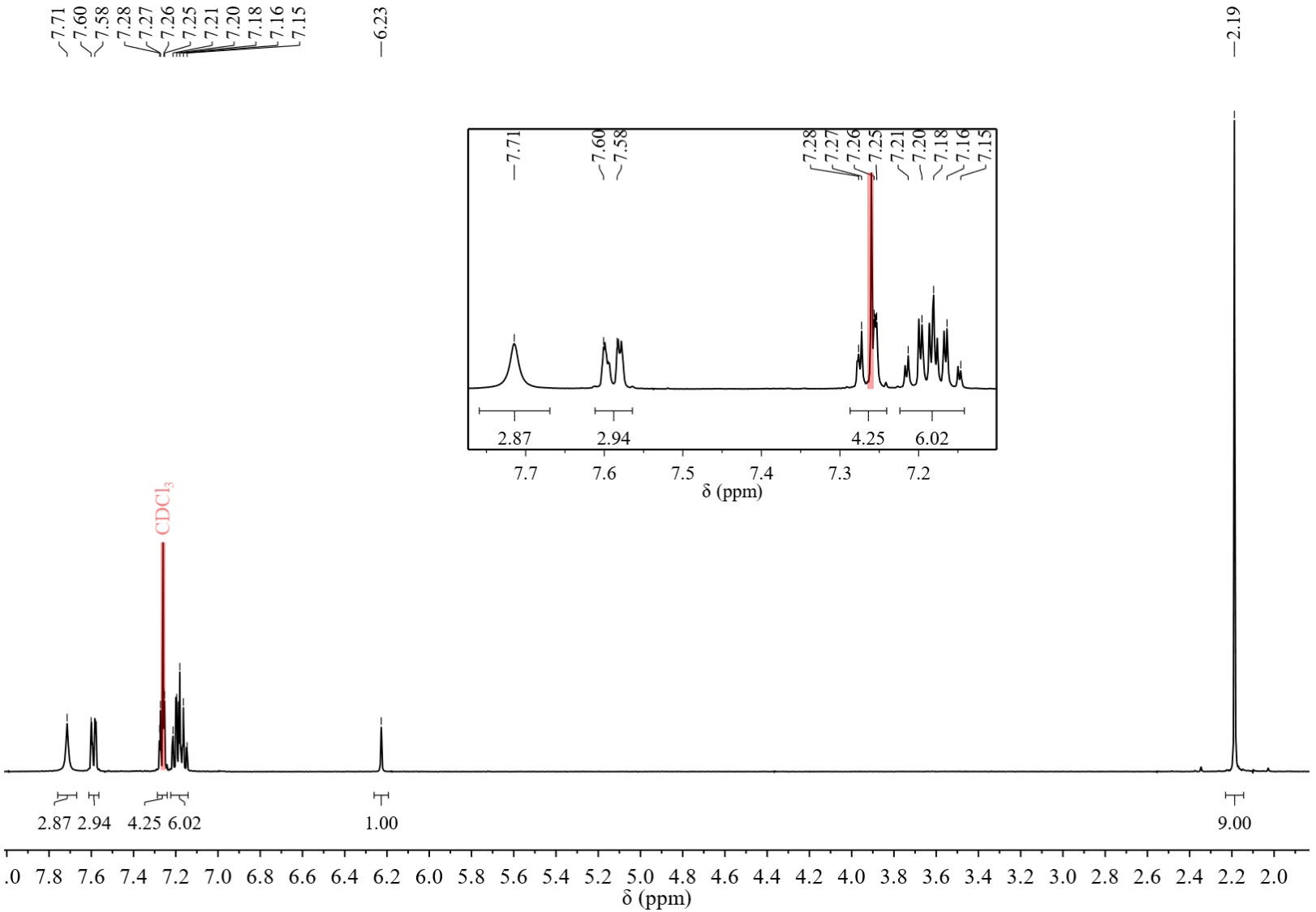

Figure S13. ^{1}H NMR of **1** in $CDCl_3$.

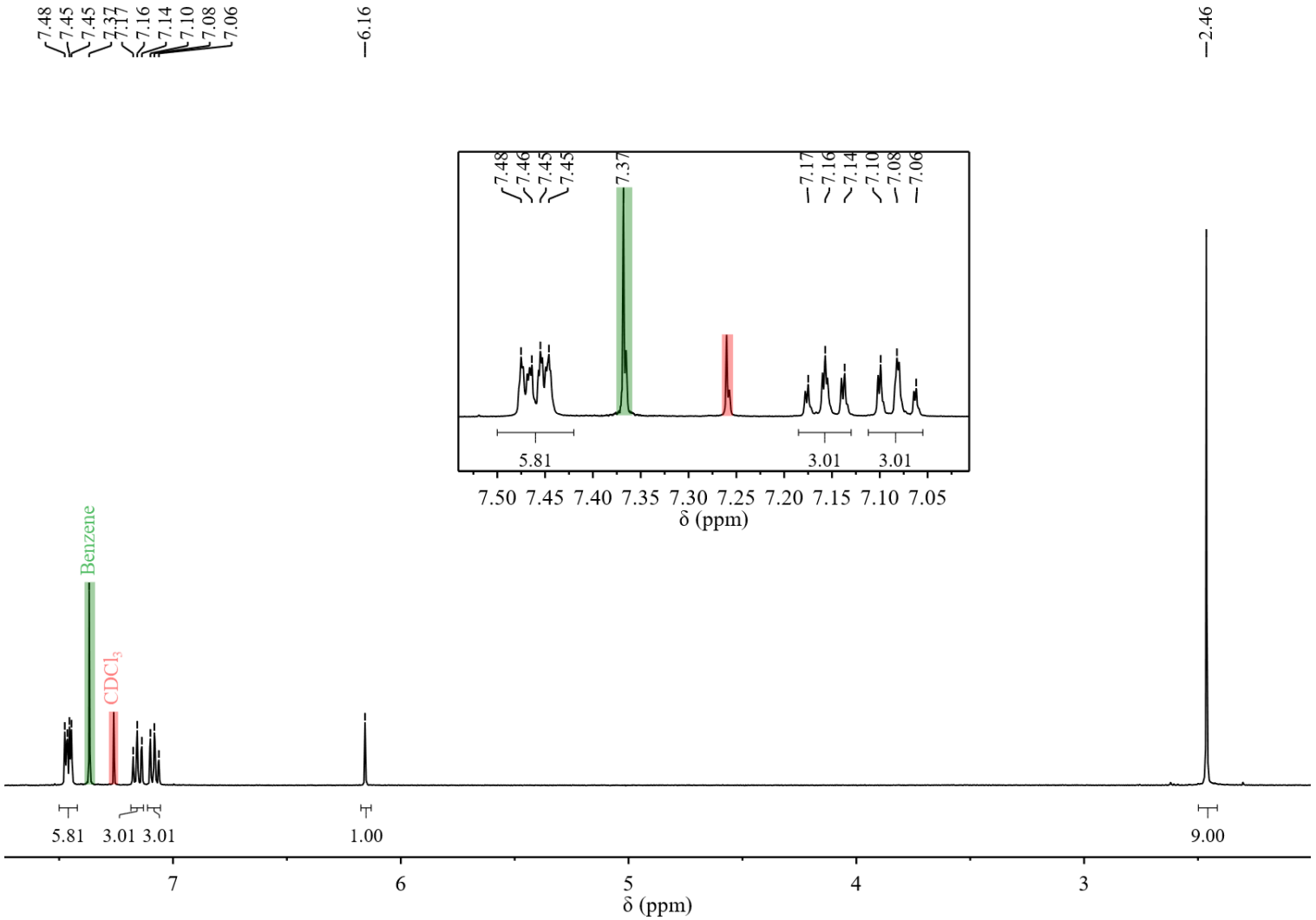

Figure S14. ^{1}H NMR of **2** in $CDCl_3$.

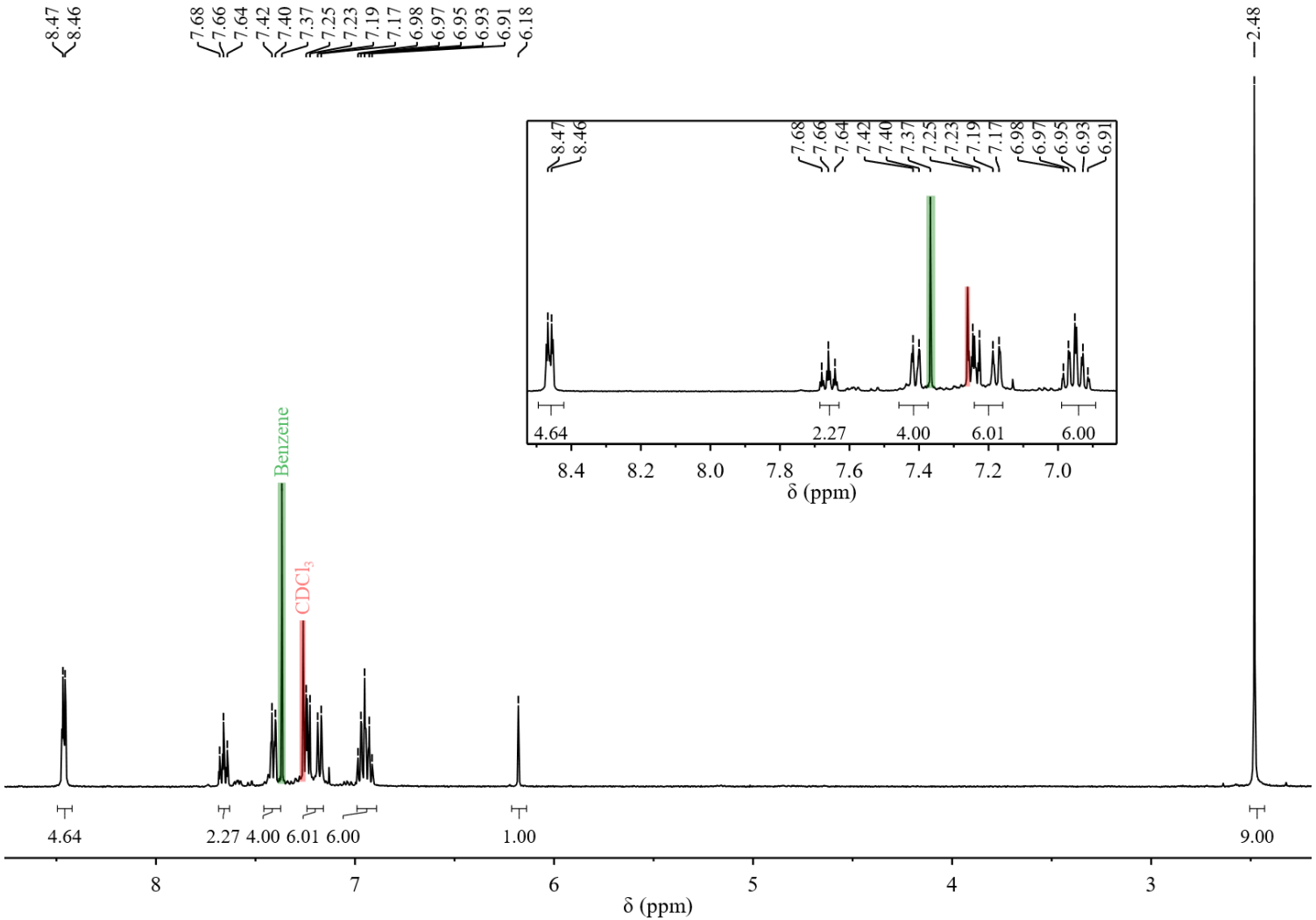

Figure S15. ^{1}H NMR of **2**·Py_2 in $CDCl_3$.

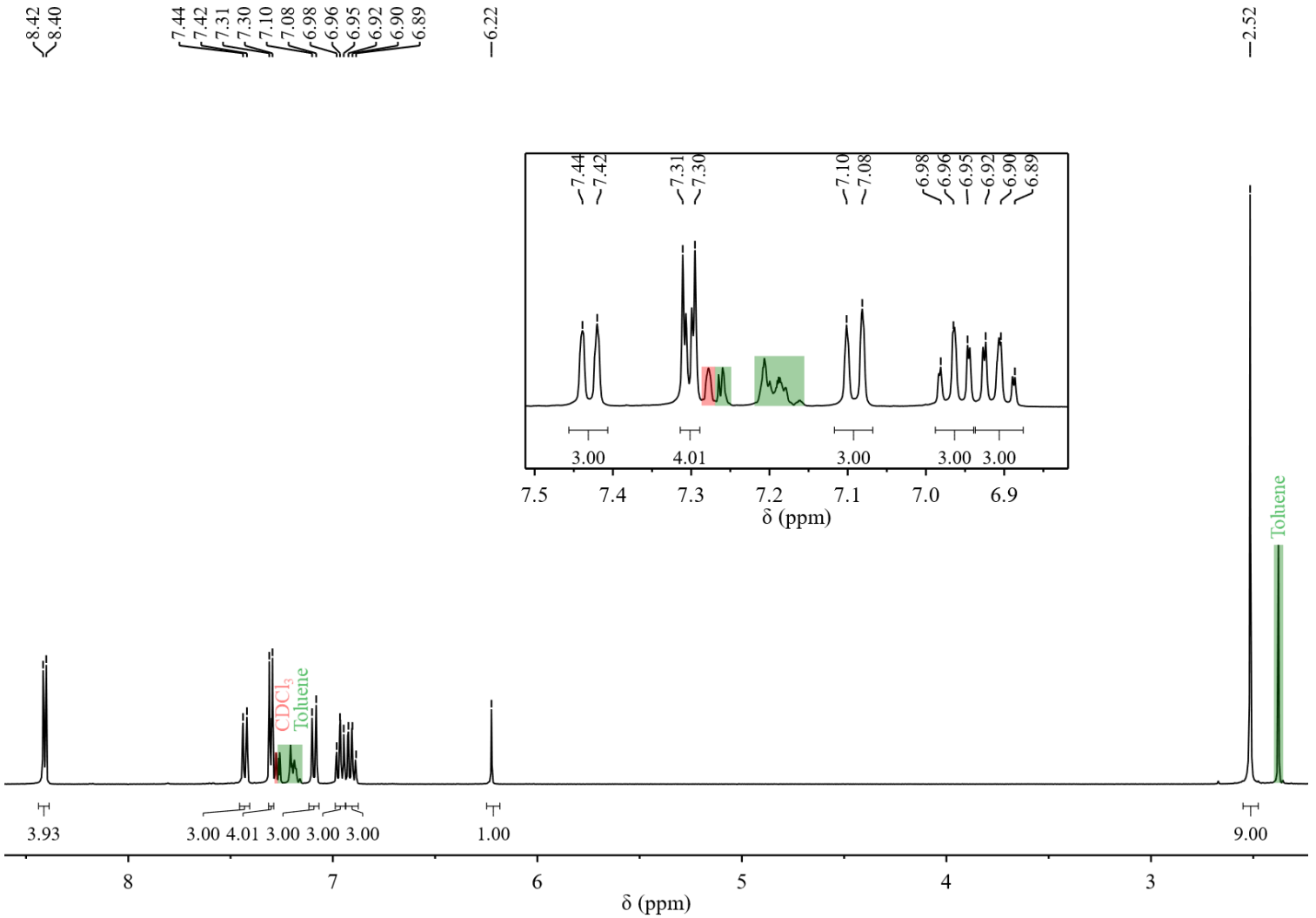

Figure S16. ^{1}H NMR of **2**·BP in $CDCl_3$.

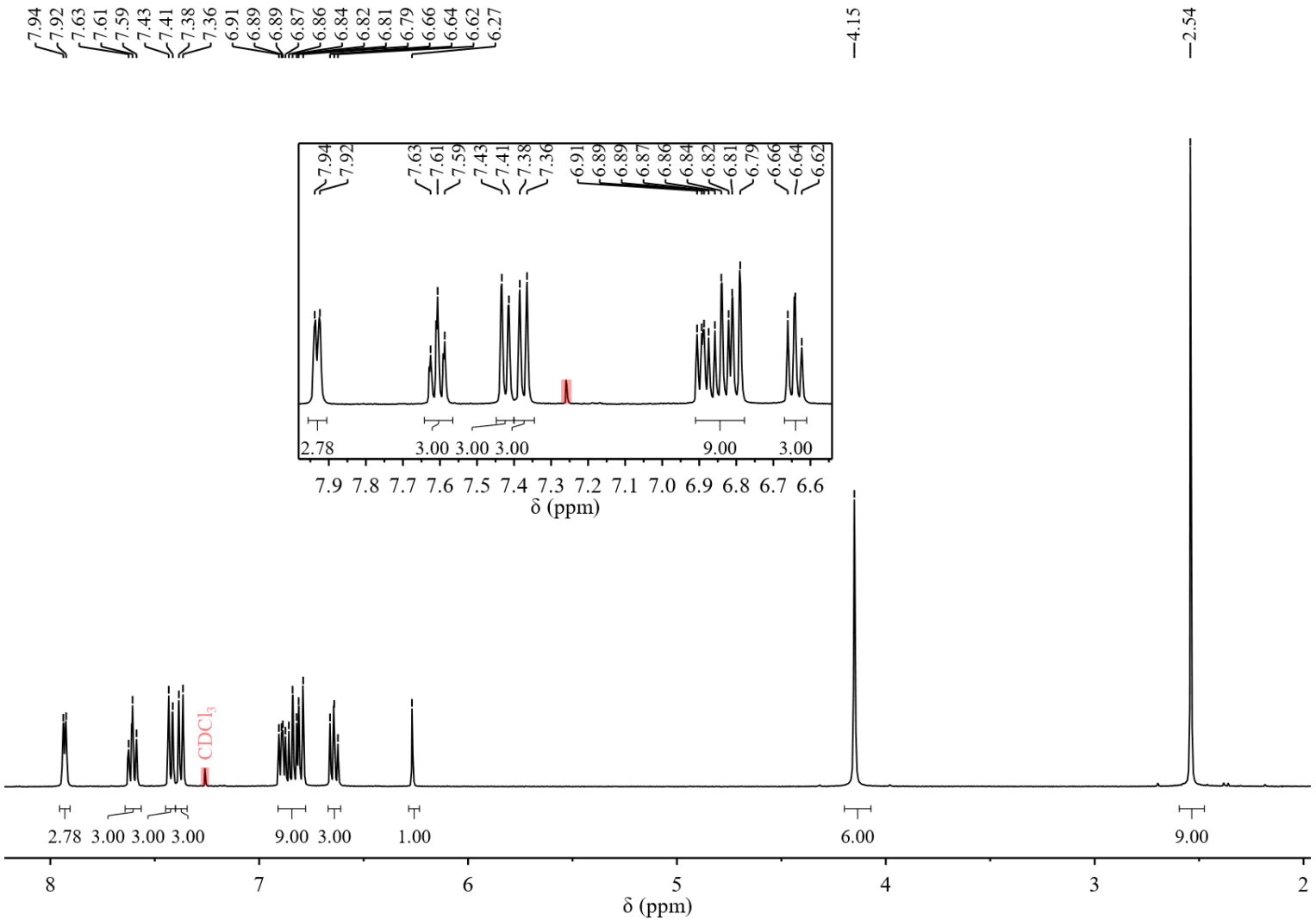

Figure S17. ^{1}H NMR of **2**·TPA in $CDCl_3$.

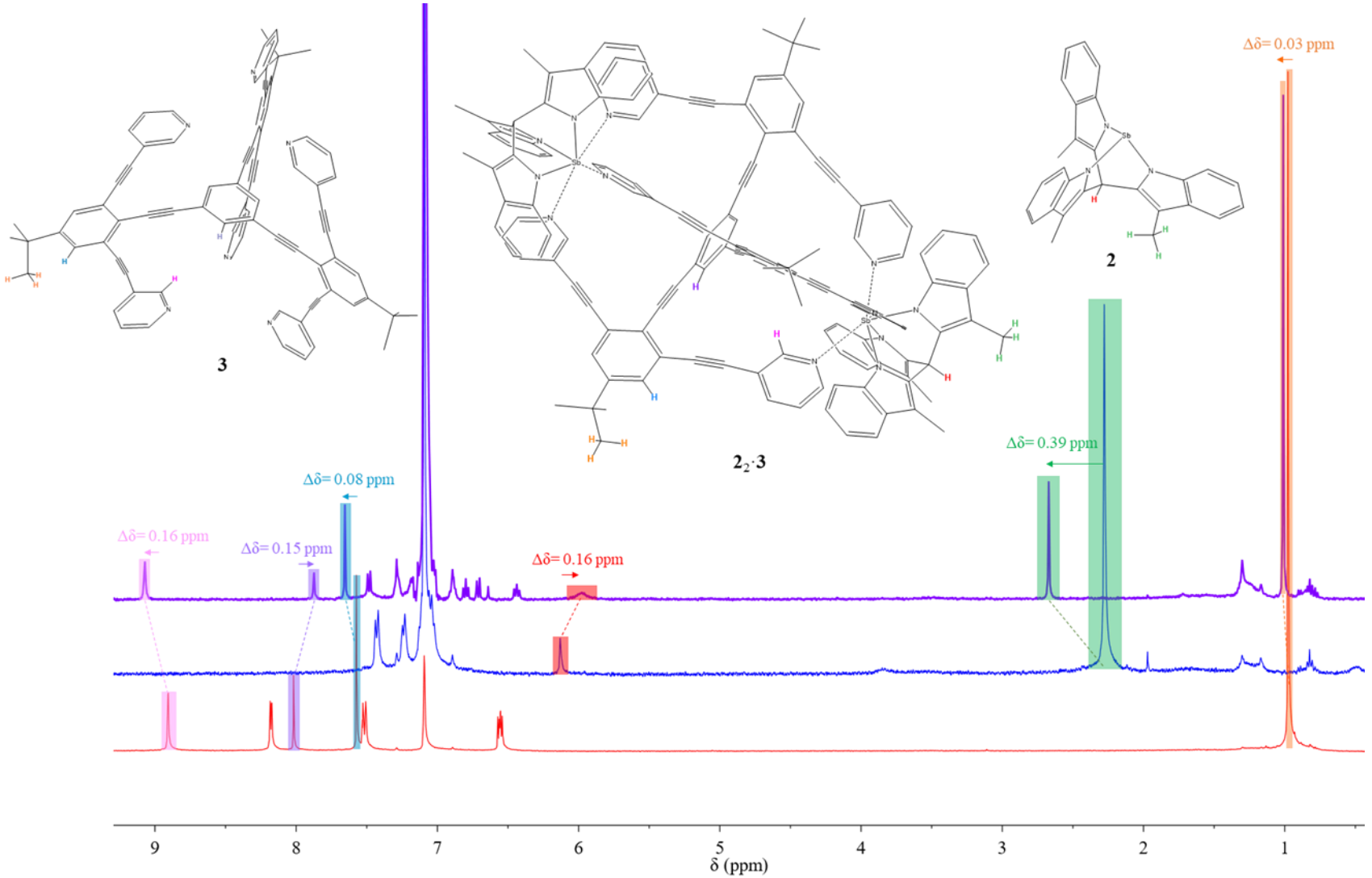

Figure S18. ^{1}H NMR of **3** (red), **2** (blue), and **2**$_2$·**3** (purple) in benzene-d_6. The difference between chemical shifts of some of the protons is indicated with its corresponding color.

S2.2 $^{13}C\{^{1}H\}$ NMR

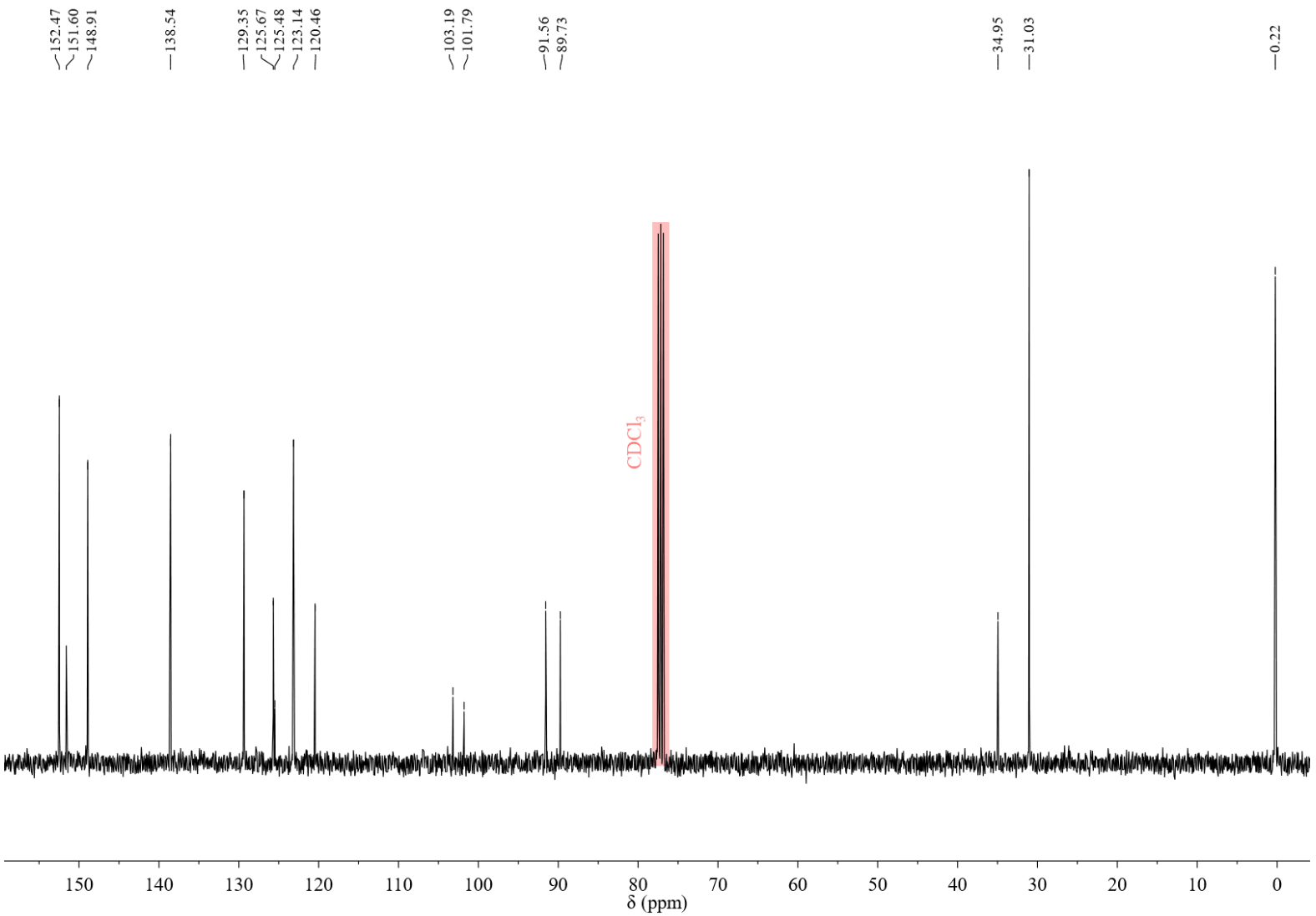

Figure S19. $^{13}C\{^{1}H\}$ NMR of **5** in $CDCl_3$.

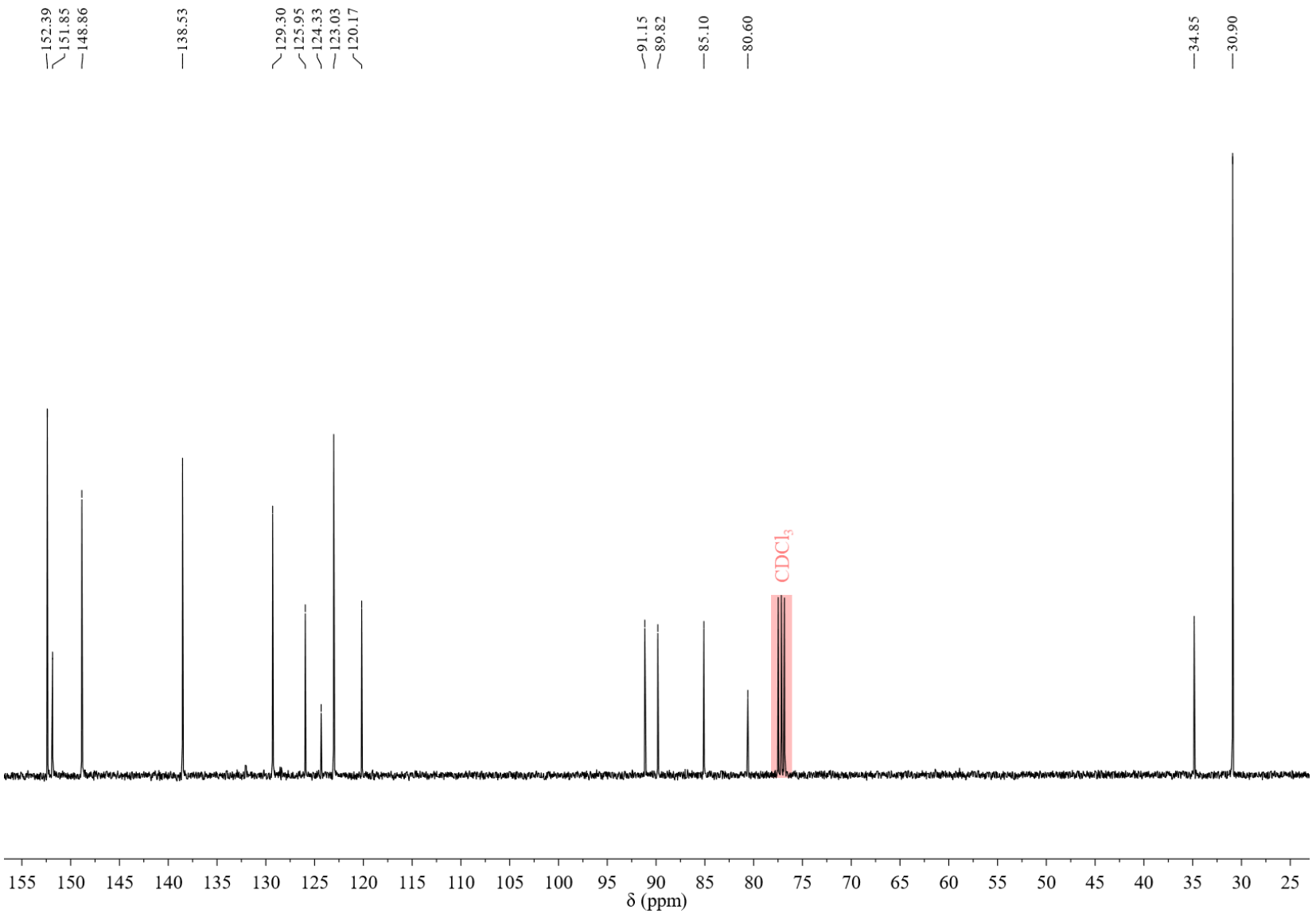

Figure S20. $^{13}C\{^{1}H\}$ NMR of **4** in $CDCl_3$.

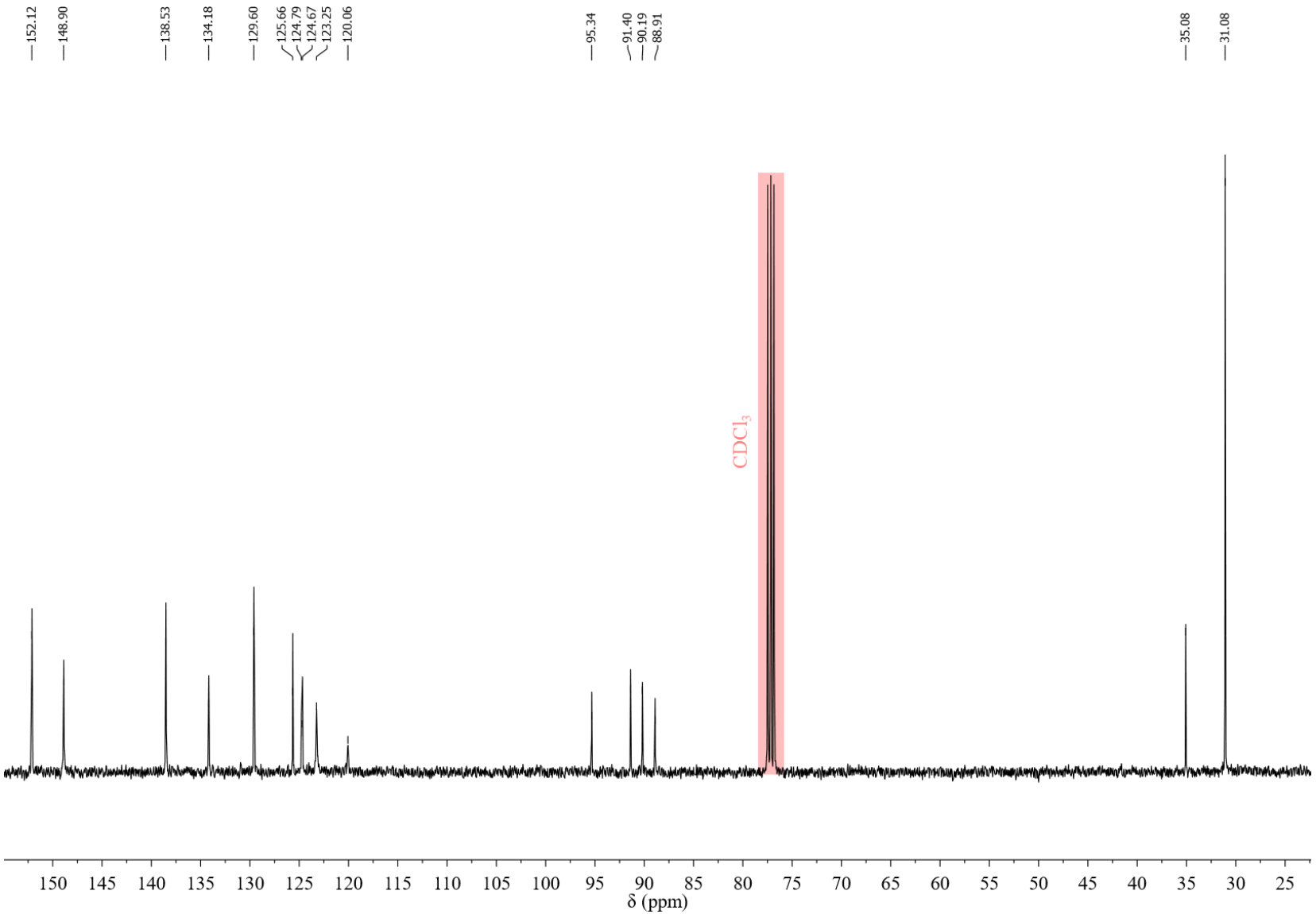

Figure S21. $^{13}C\{^{1}H\}$ NMR of **3** in $CDCl_3$.

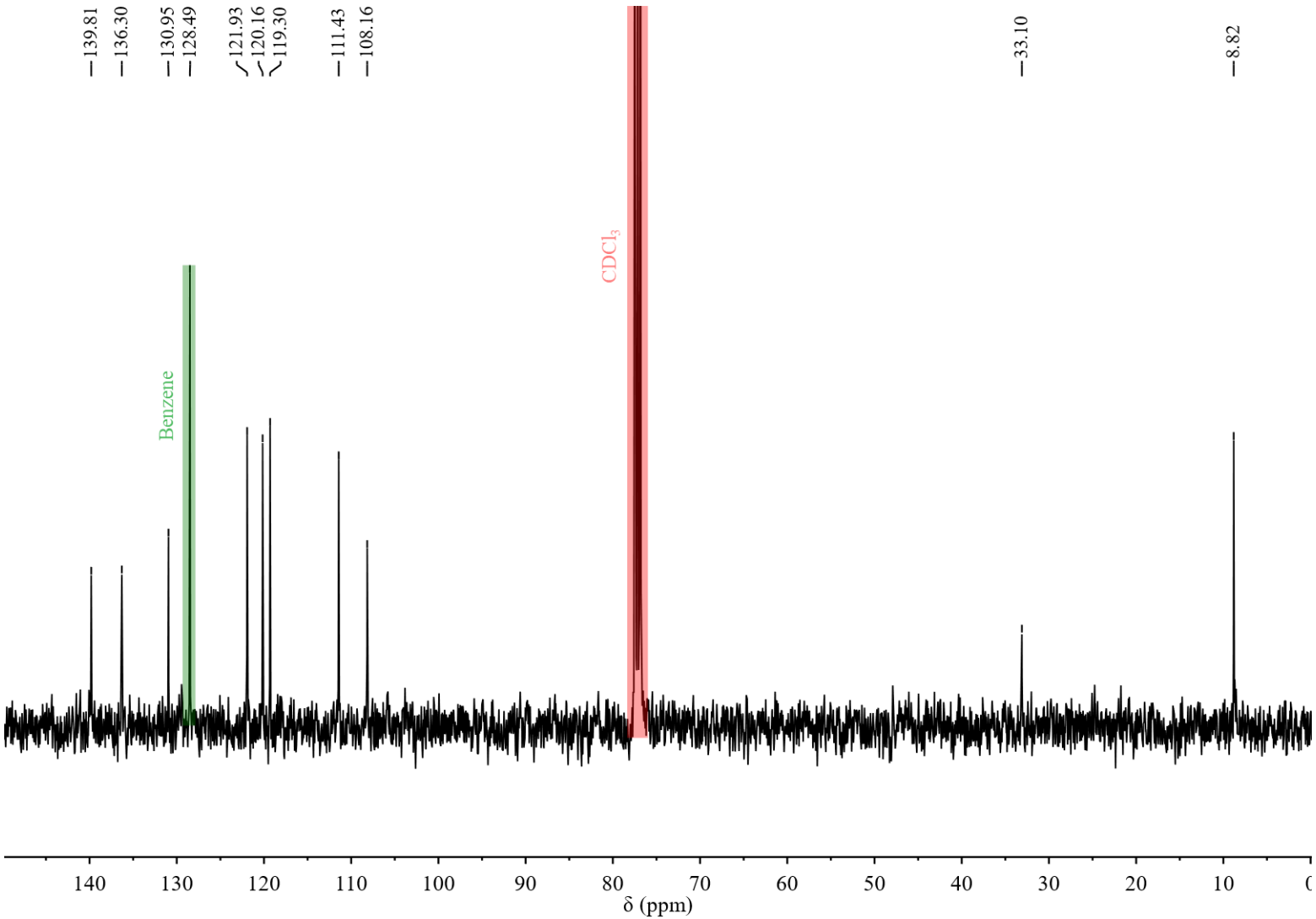

Figure S22. $^{13}C\{^{1}H\}$ NMR of **2** in $CDCl_3$.

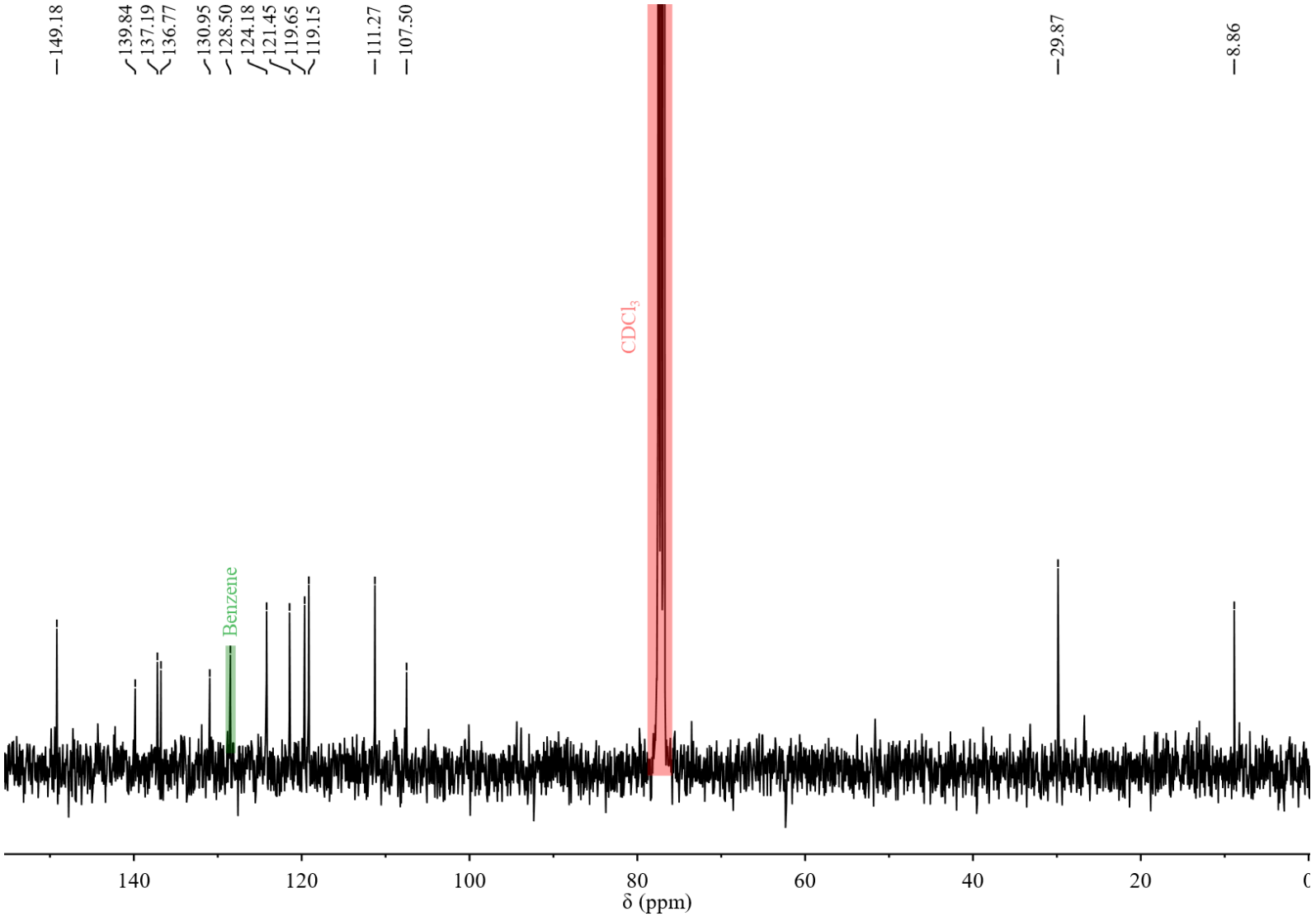

Figure S23. $^{13}C\{^{1}H\}$ NMR of **2**·Py_2 in $CDCl_3$.

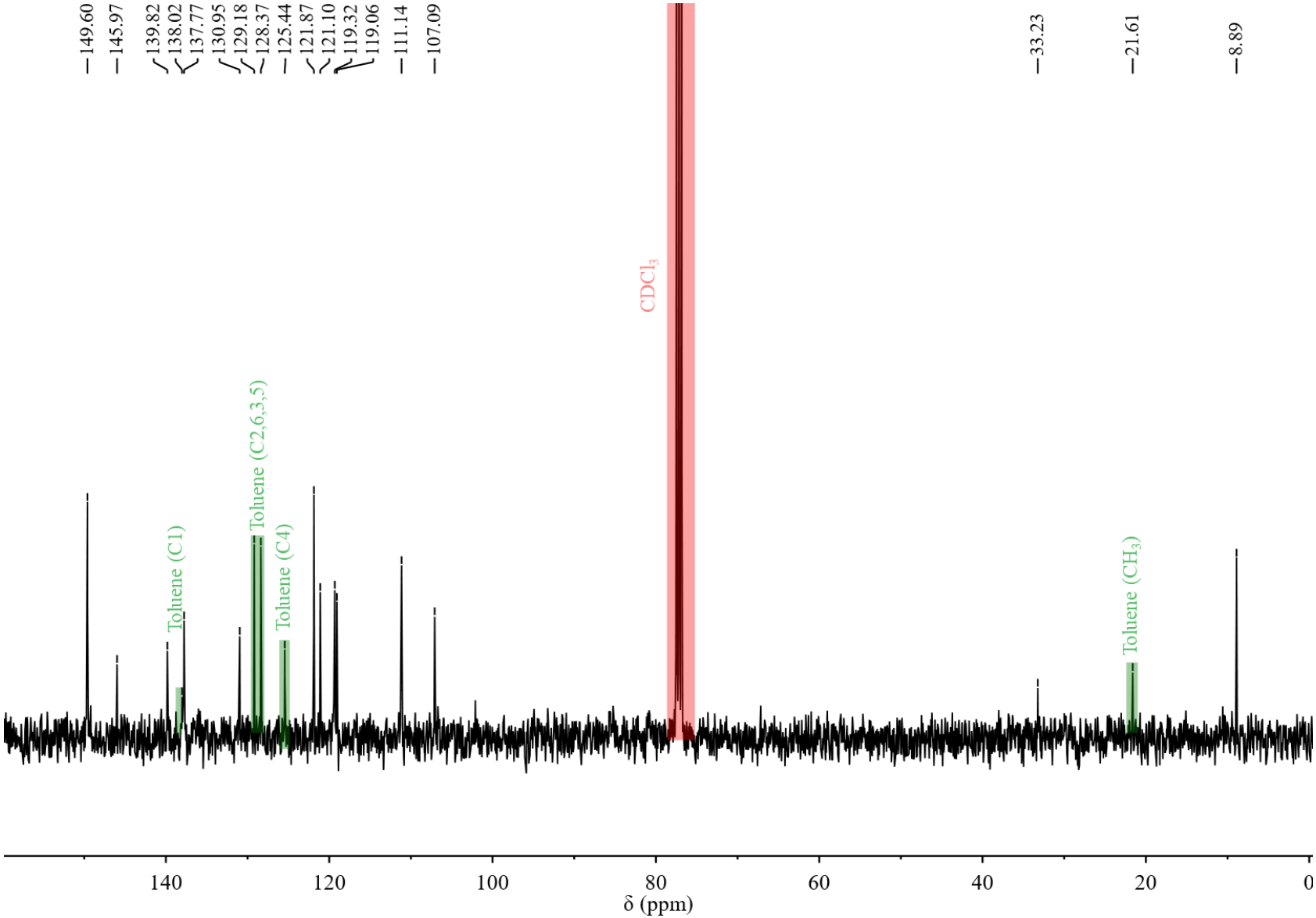

Figure S24. $^{13}C\{^{1}H\}$ NMR of **2**·BP in $CDCl_3$.

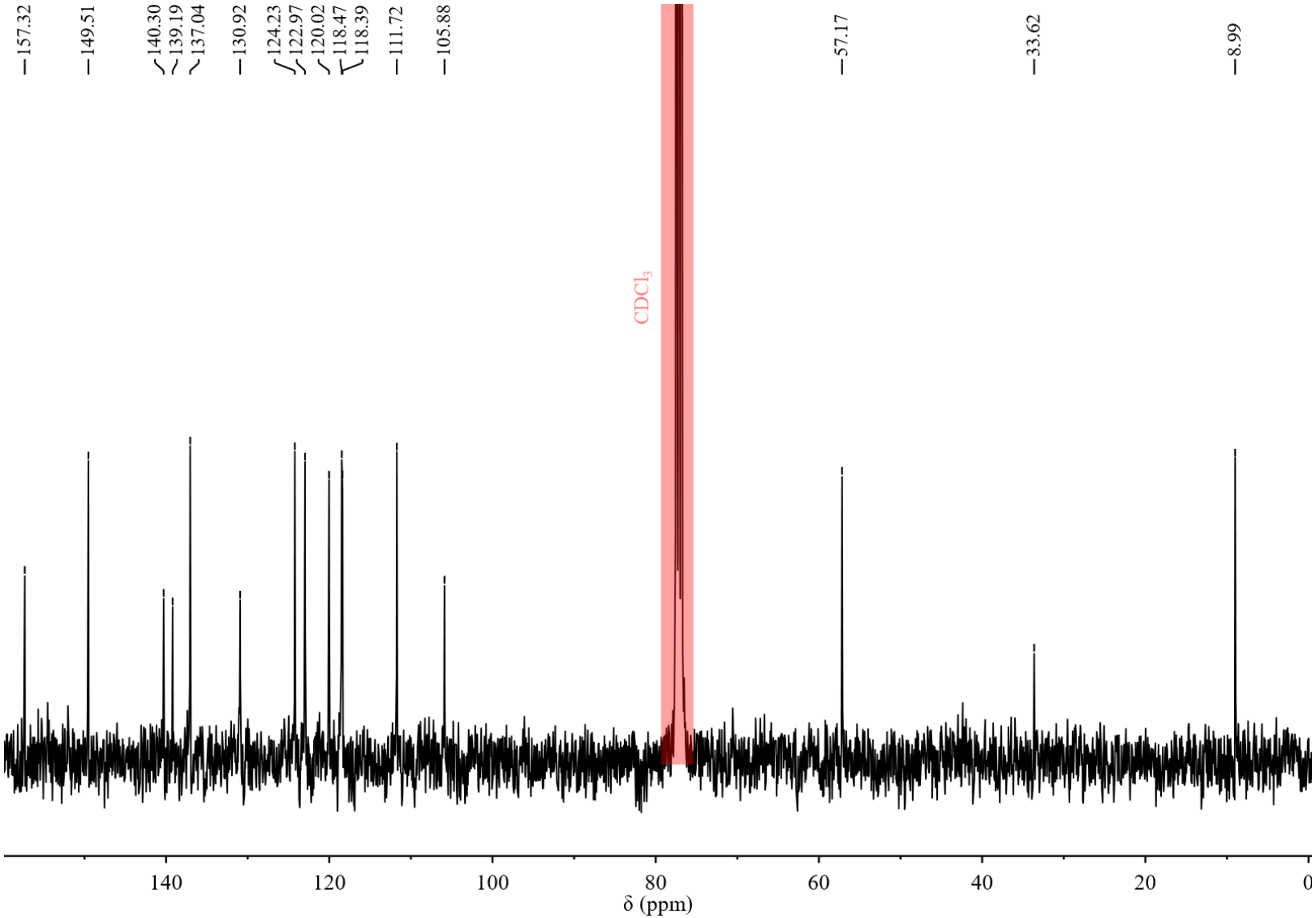

Figure S25. $^{13}C\{^{1}H\}$ NMR of **2**·TPA in $CDCl_3$.

S2.3 ATR-FTIR

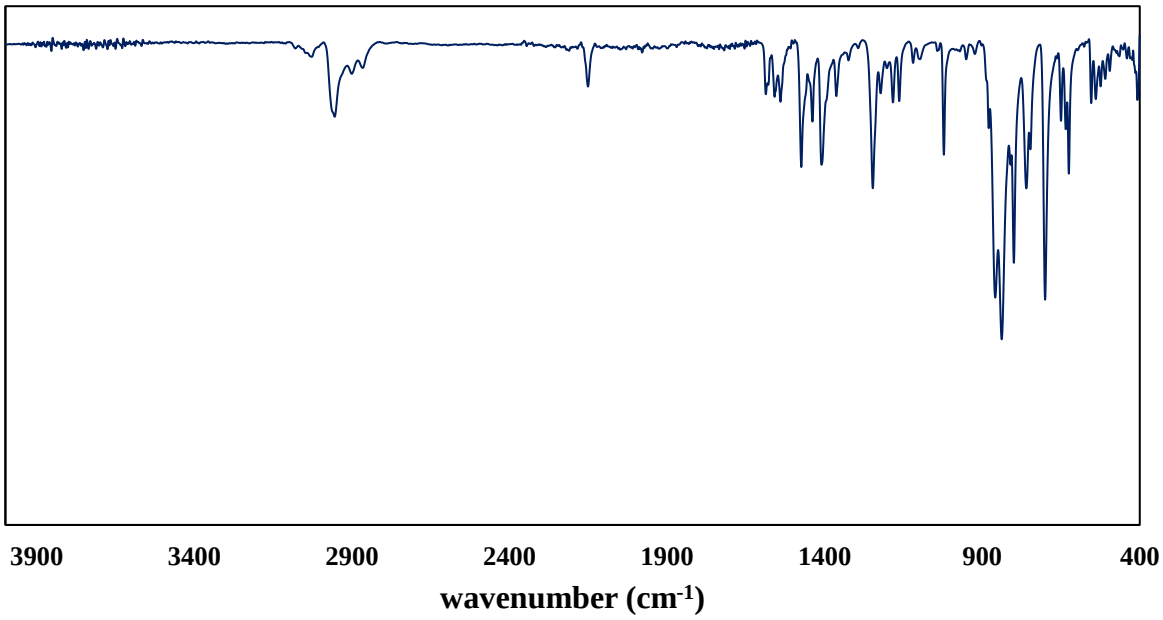

Figure S26. Di-ATR FTIR of **5**.

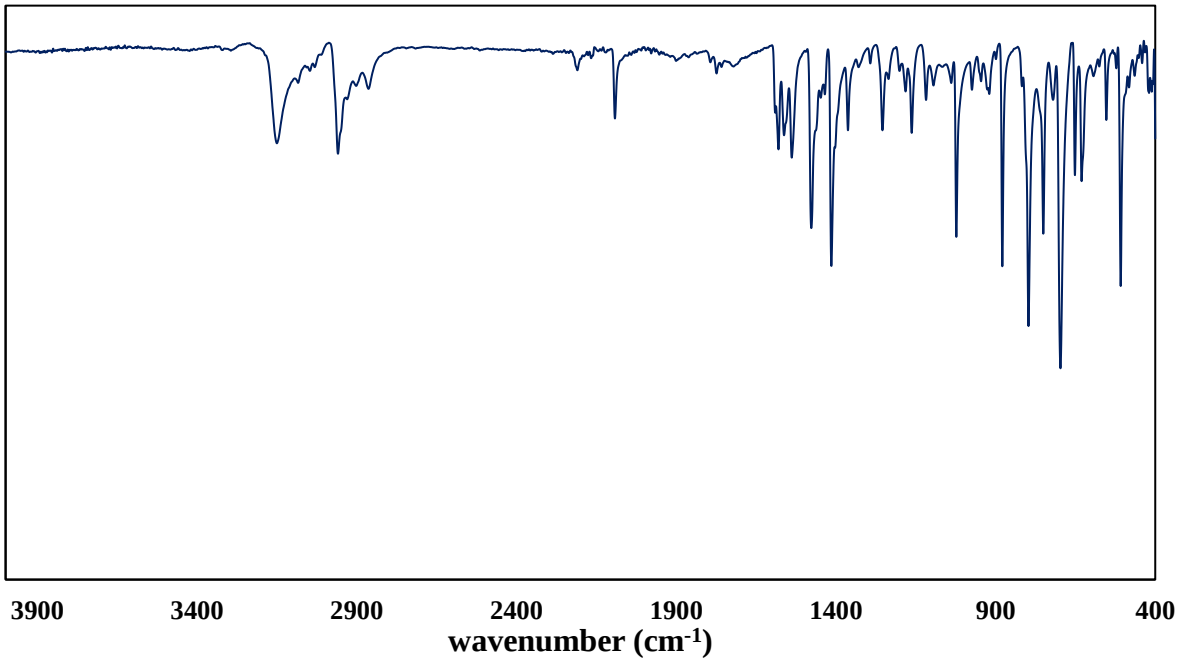

Figure S27. Di-ATR FTIR of **4**.

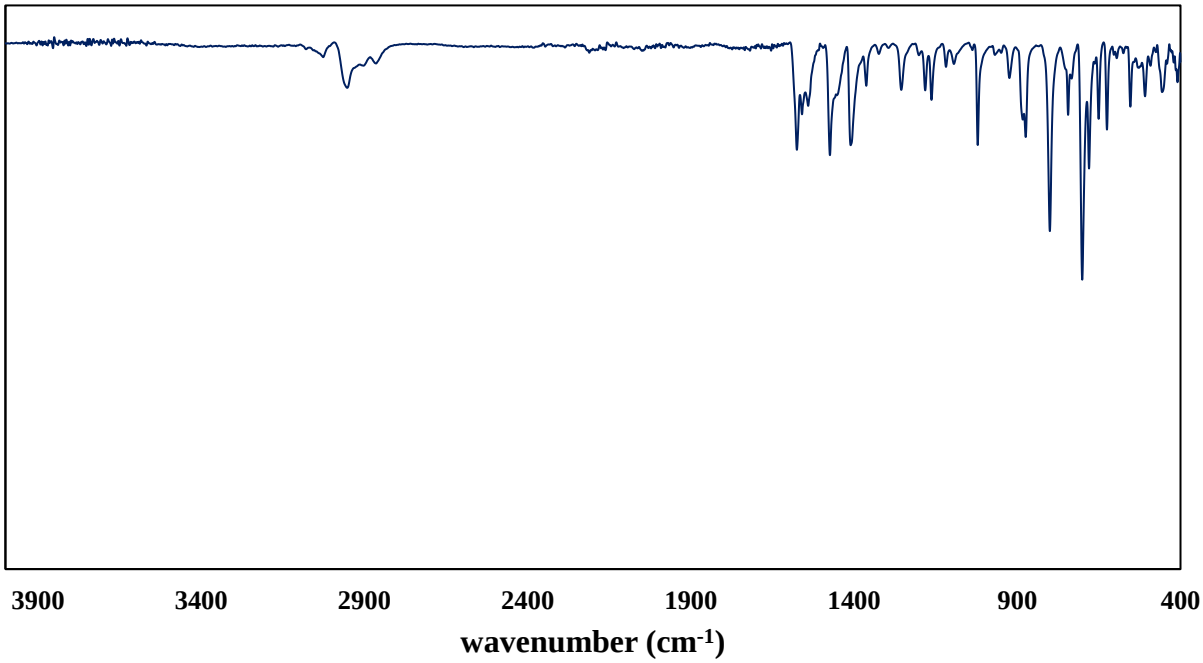

Figure S28. Di-ATR FTIR of **3**.

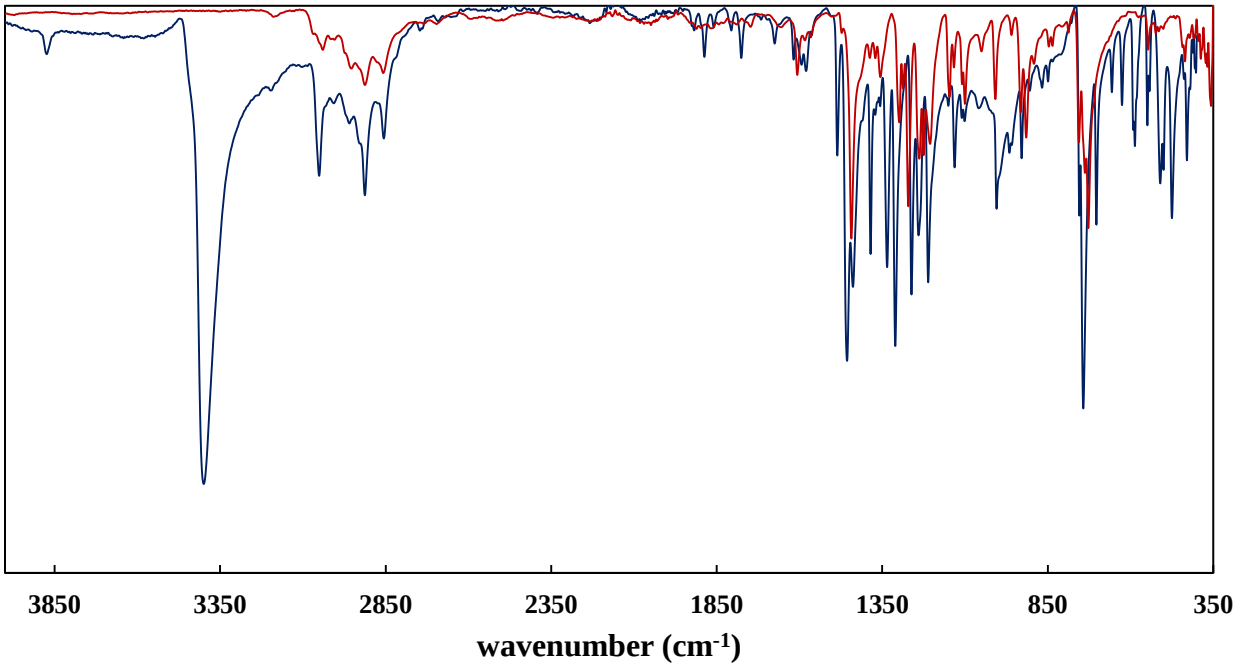

Figure S29. Di-ATR FTIR of **1**(blue) and **2** (red).

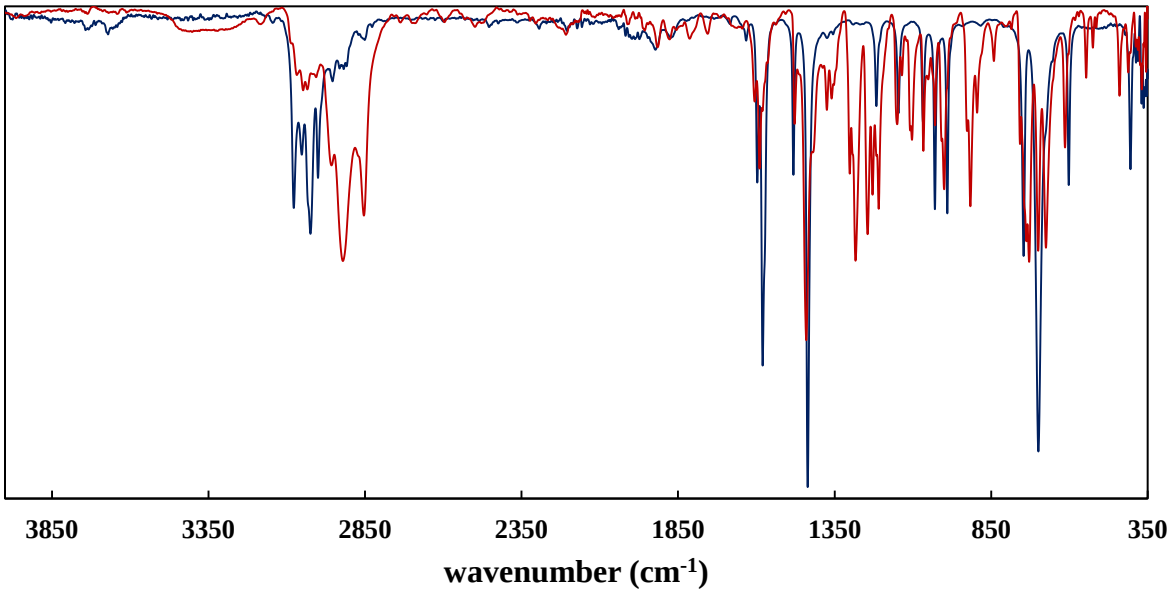

Figure S30. Di-ATR FTIR of Pyridine (blue) and **2**·Py_2 (red).

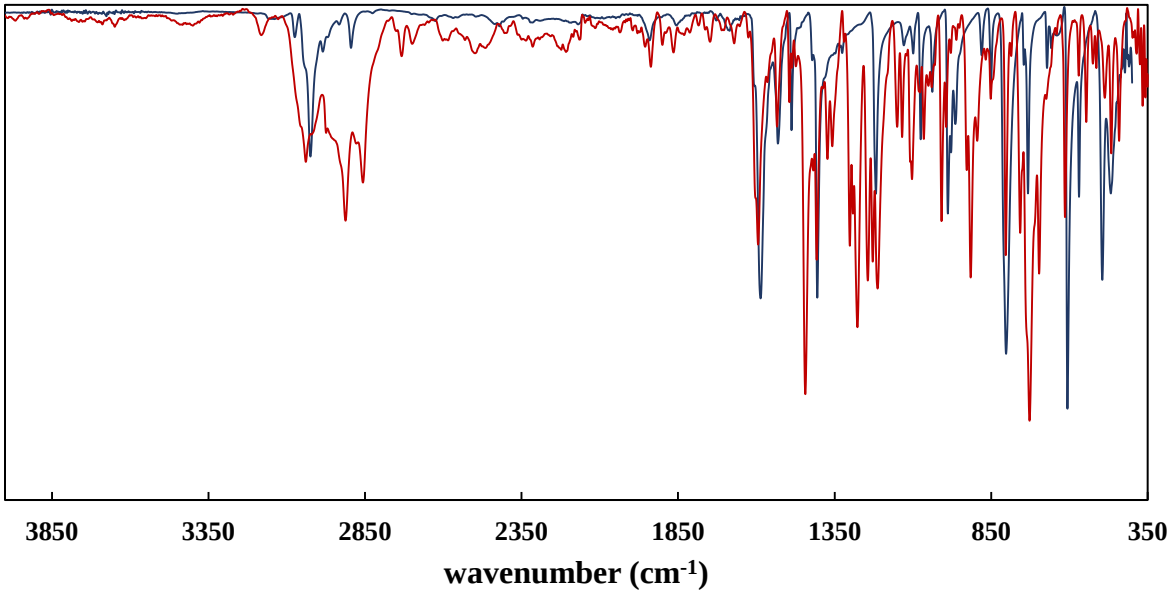

Figure S31. Di-ATR FTIR of BP (blue) and **2**·BP (red).

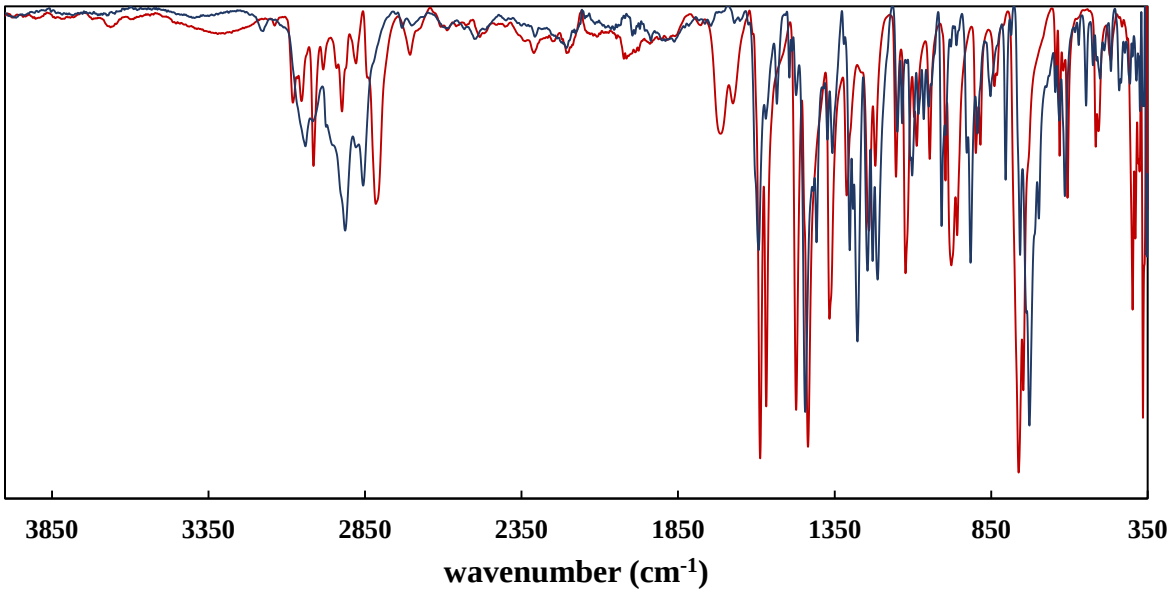

Figure S32. Di-ATR FTIR of TPA (red) and **2**·TPA (blue).

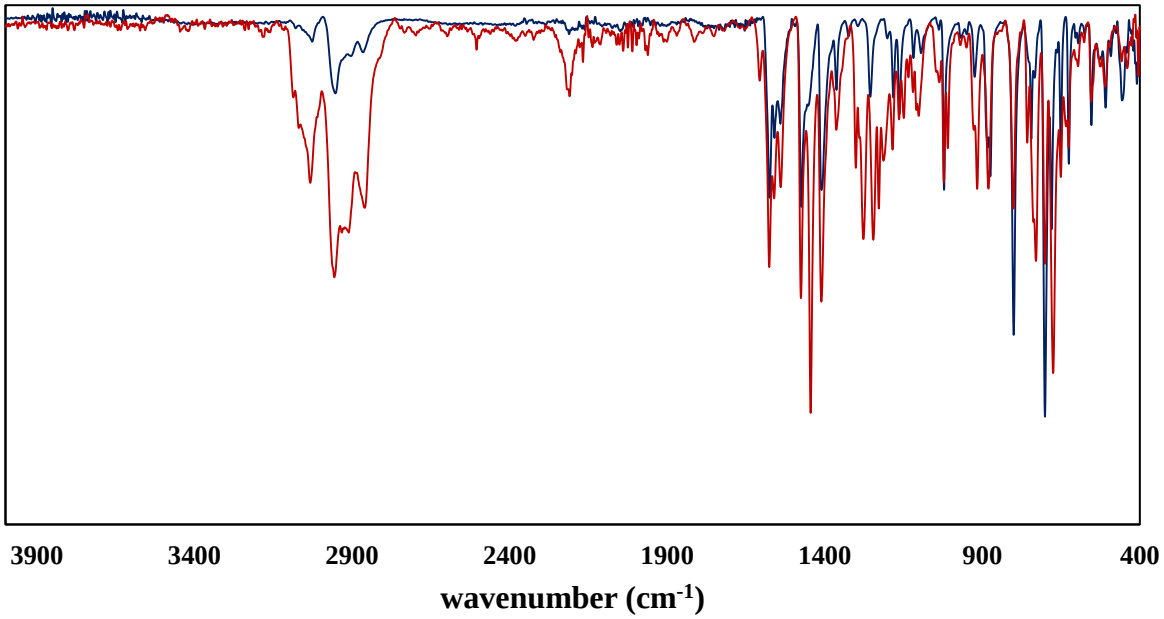

Figure S33. Di-ATR FTIR of $\mathbf{2}_2$·**3** (red) and **3** (blue).

S2.4 PXRD

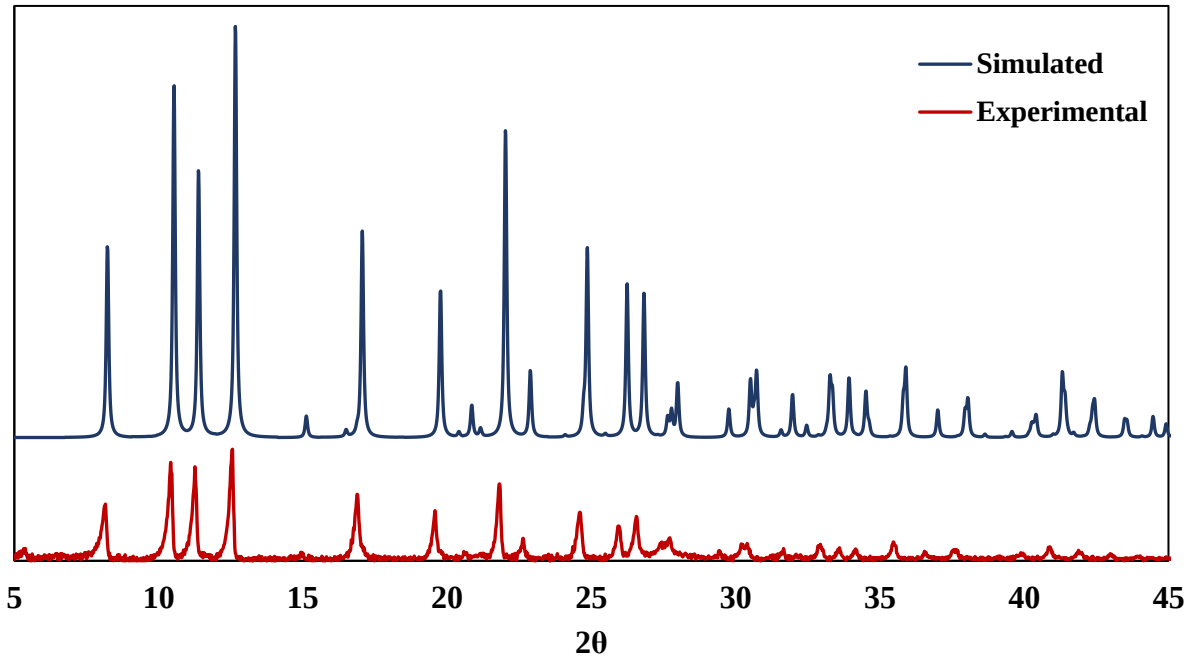

Figure S34. PXRD of **2**·½C_6H_6.

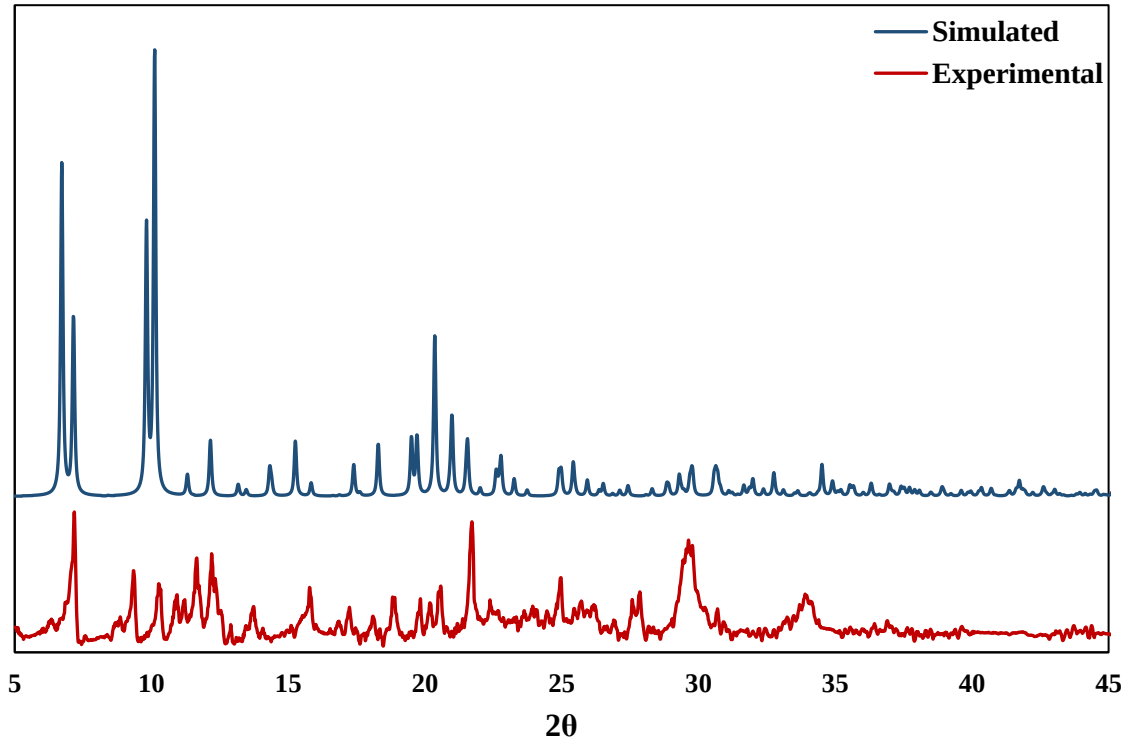

Figure S35. PXRD of **2**·Py_2.

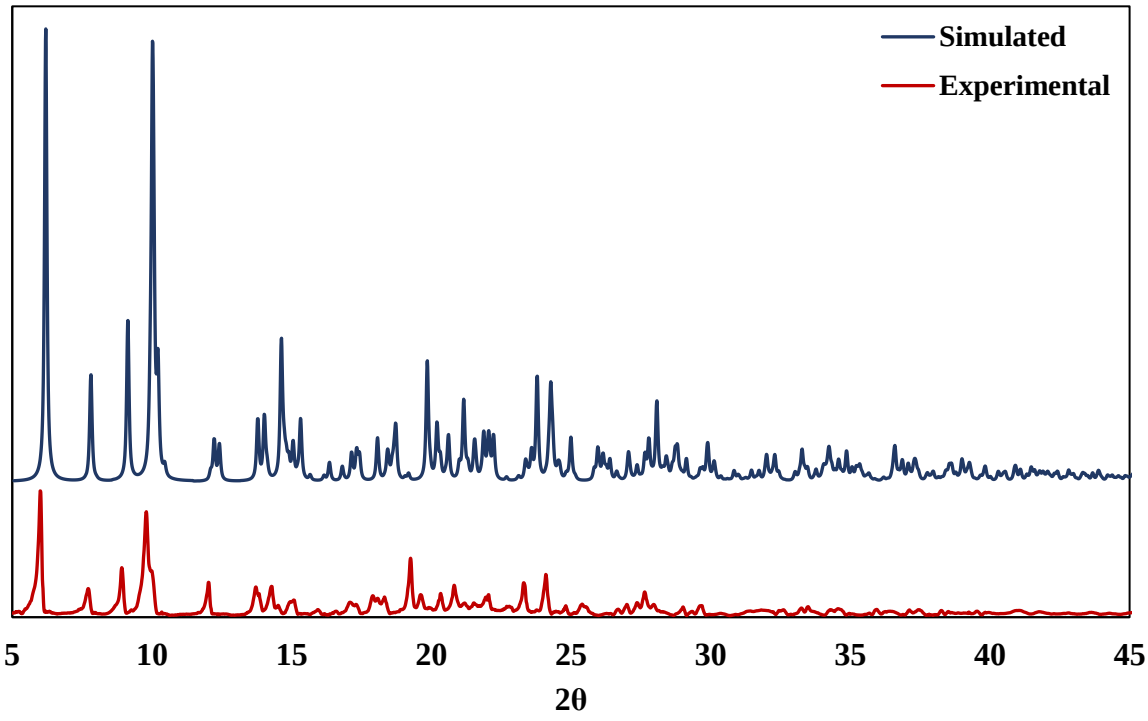

Figure S36. PXRD of **2**·BP.

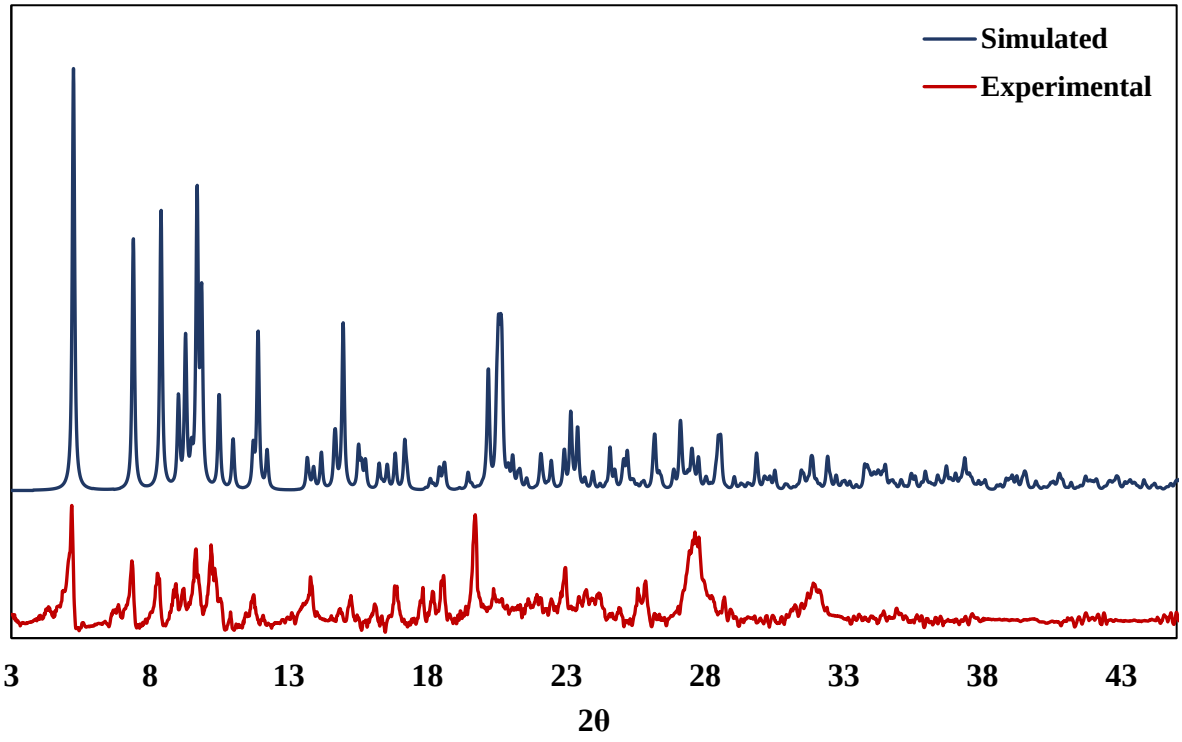

Figure S37. PXRD of **2**·TPA.

S3 Solution-State Binding Studies

S3.1 UV/vis Titrations

S3.1.1 Titration Data Collection

UV-vis spectra were collected on a Silver-Nova Super Range TEC spectrometer, with SL1 Tungsten Halogen Lamp (visible and near-IR region) and SL3 Deuterium Lamp (UV region) as the light source. The spectrometer was equipped with a CUV-TEMP cuvette holder (qpod 2e) with a path length of 1.0 cm. All spectra were collected at 293 K with a stir rate of 1200 rpm.

Before each data collection trial, dark and blank (of pure, dry dichloromethane) spectra were collected. Under inert, dry atmosphere, 2.00 mL of the solution of **2** (approximate concentrations of 20 μM) was loaded via syringe into the cuvette that was charged with a stir bar and capped with a custom Teflon cap, with a small hole drilled through it, just large enough for the needle of the syringe (vide infra). Each pyridine receptor solution was loaded into a 25.0 μL Hamilton 80200 gastight syringe (with cemented needle). The syringe was used along with a Hamilton PB600-1 repeating dispenser. This assembly dispenses the volume of the syringe in 50 identical increments; under these conditions, each press of the button dispenses 0.500 μL of the pyridine receptor solution. Solutions of varying concentrations of pyridine receptor solutions were made such that three consecutive receptor solutions could be added per titration. This enabled control over the number of data points, particularly fewer equivalents of pyridine receptor. Approximate concentrations of 2, 8, and 80 mM pyridine receptor solutions were used in succession, starting with the least concentrated and working up to the most concentrated to minimize the effect of contamination of the syringe.

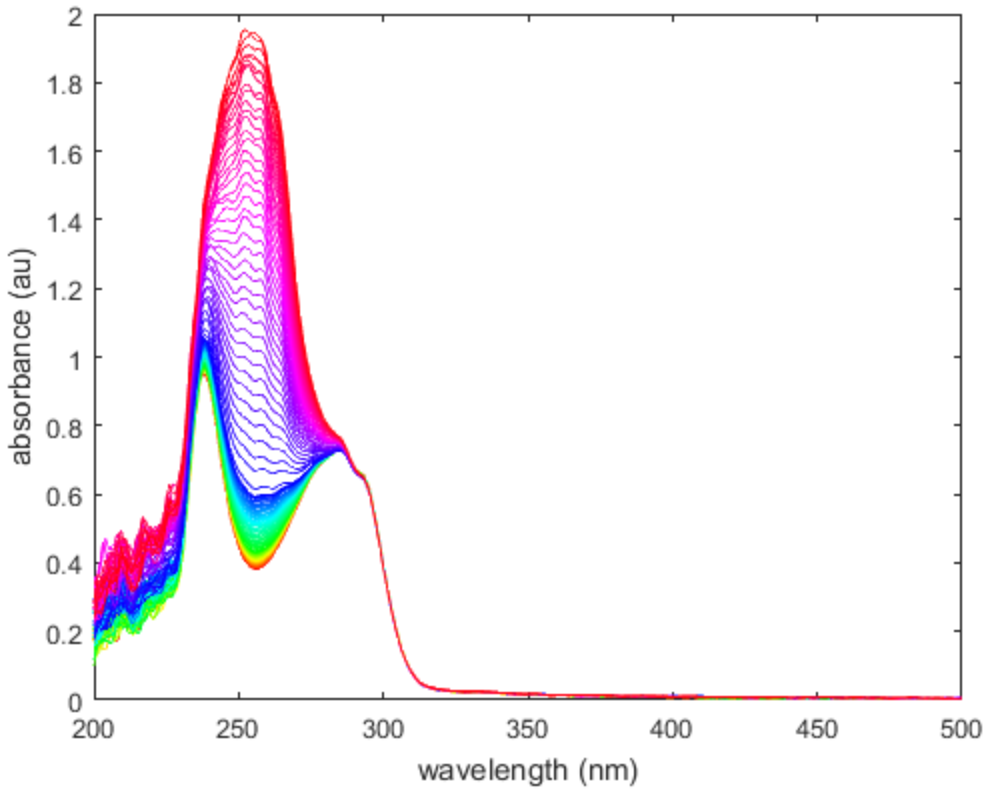

Figure S38. UV-vis spectra of titration of 26.4 μM **2** with solutions of pyridine (2.03 mM, 7.50 mM, and 88.6 mM) in DCM.

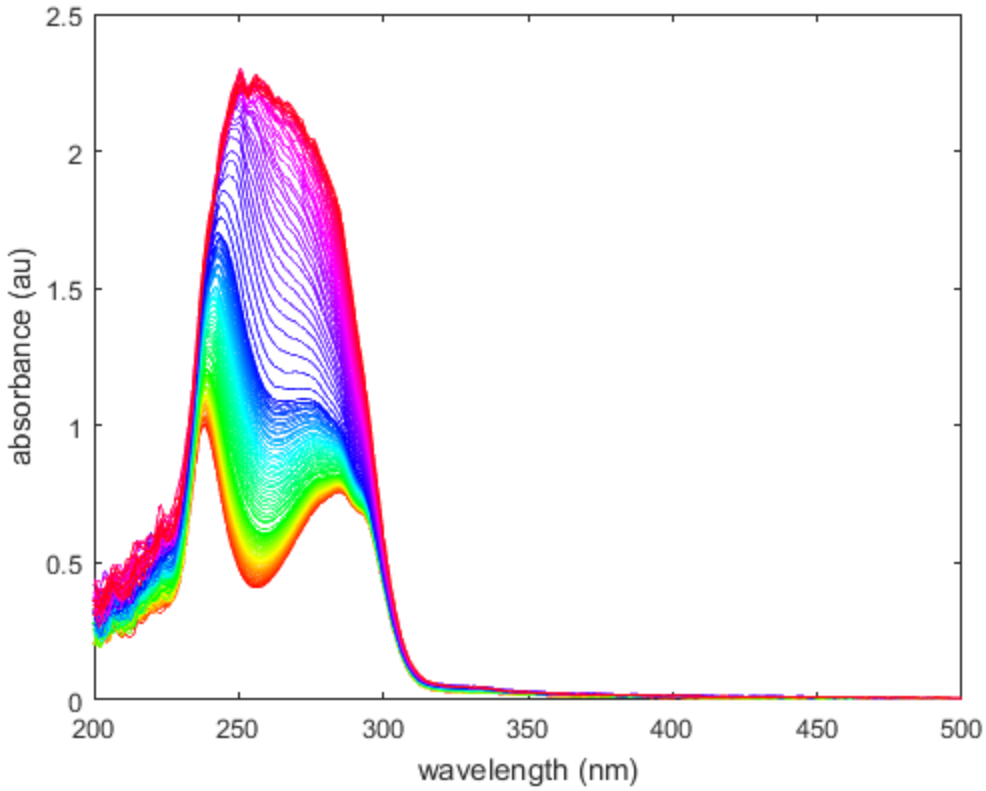

Figure S39. UV-vis spectra of titration of 26.4 μM **2** with solutions of 4,4′–pyridine (2.21 mM, 7.22 mM, and 49.5 mM) in DCM.

S3.1.2 Data Fitting

The intensity data from the wavelength that has the largest change over the course of the titration (without exceeding an absorbance of 1) was fitted against modeled data. The models that were used have been described previously.[21] For each set of data, the 1:1 binding model was first applied. One hundred possible solutions were obtained from randomly chosen starting points for each parameter. The residuals were analyzed to ensure that the model was correct as verified by a stochastic distribution. The data was also fitted to a composite binding model that included equilibria for 1:1 binding and 1:2 binding. The residuals for this model had a similar stochastic distribution to those of the 1:1 model, and the RMS values for the composite model indicated that it was not a better fit than the 1:1 model. Errors were determined by bootstrapping. The data was resampled 100 times for each trial with a sample size equal to the number of datapoints collected

for each trial. The trials were then averaged together and the maximum error (from bootstrap or trial averaging) was reported. In the case of the ditopic **BP** receptor, an additional binding model that included equilibria for 2:1 (**2**:**BP**) and 1:1 binding. Even though this model gave a reasonable fit similar to that of 1:1 binding (Figure S42), the residuals from the difference between this model and the experimental data deviated more than those of the 1:1 model, so the 1:1 model was used.

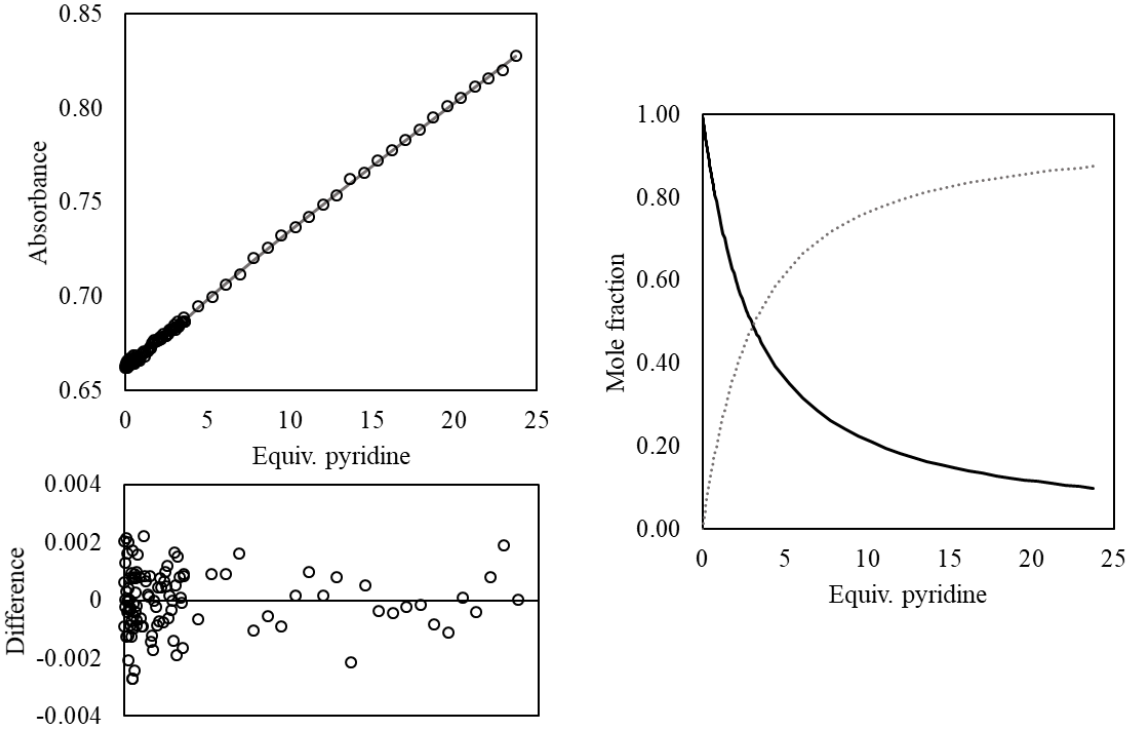

Figure S40. Titration data for **2** with pyridine fitted to a 1:1 binding model, monitored at 276 nm with residuals (left, solid line represents model) and speciation diagram (right, solid line is **2**, dotted line is 1:1 complex).

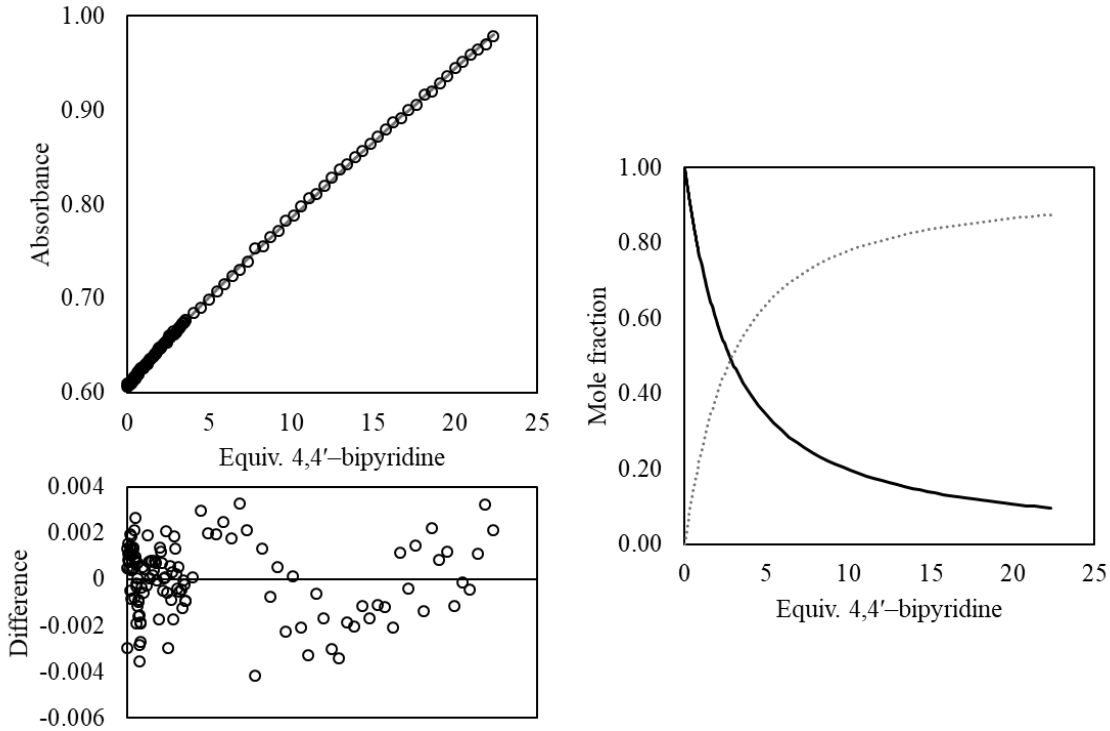

Figure S41. Titration data for **2** with 4,4′–bipyridine fitted to a 1:1 binding model, monitored at 296 nm with residuals (left, solid line represents model) and speciation diagram (right, solid line is **2**, dotted line is 1:1 complex).

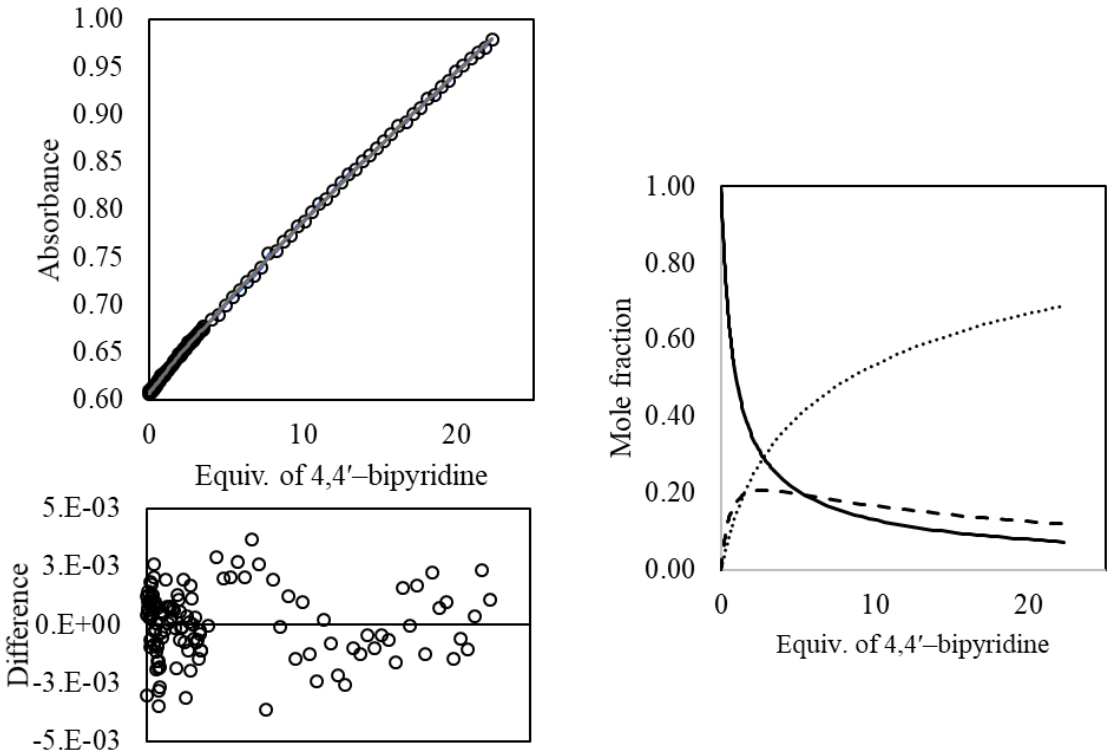

Figure S42. Titration data for **2** with 4,4′–bipyridine fitted to a 2:1 and 1:1 composite binding model, monitored at 296 nm with residuals (left, solid line represents model) and speciation diagram (right, solid line is **2**, dotted line is 1:1 complex, hashed line is the 2:1 complex).

S3.2 Pulsed-field gradient spin echo (PFGSE) NMR spectroscopy

All diffusion constant measurements were obtained on a JEOL ESC 400 MHz NMR spectrometer in benzene-d6 solution. Spectra from the simulated spin-echo attenuation of the ^{1}H diffusion in the solution were collected with 21 gradient values from 300 to 2500 G.cm^{-1}, applied during δ= 2 ms, and 200 ms diffusion delay time. Diffusion curves were obtained from the integrated values of appropriate proton resonances and the integrated values were normalized to percent values based on the highest value. These values were fit with a diffusion model using the GRG Nonlinear engine of the Solver package in Microsoft Excel.

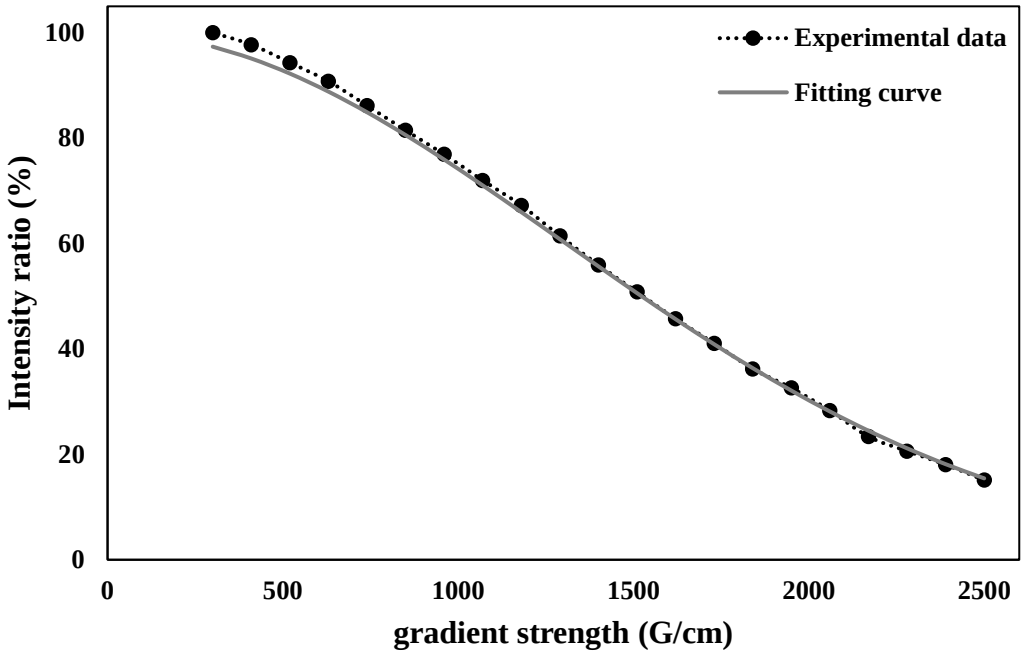

Figure S43. Fitting of **2**-Me PFGSE data.

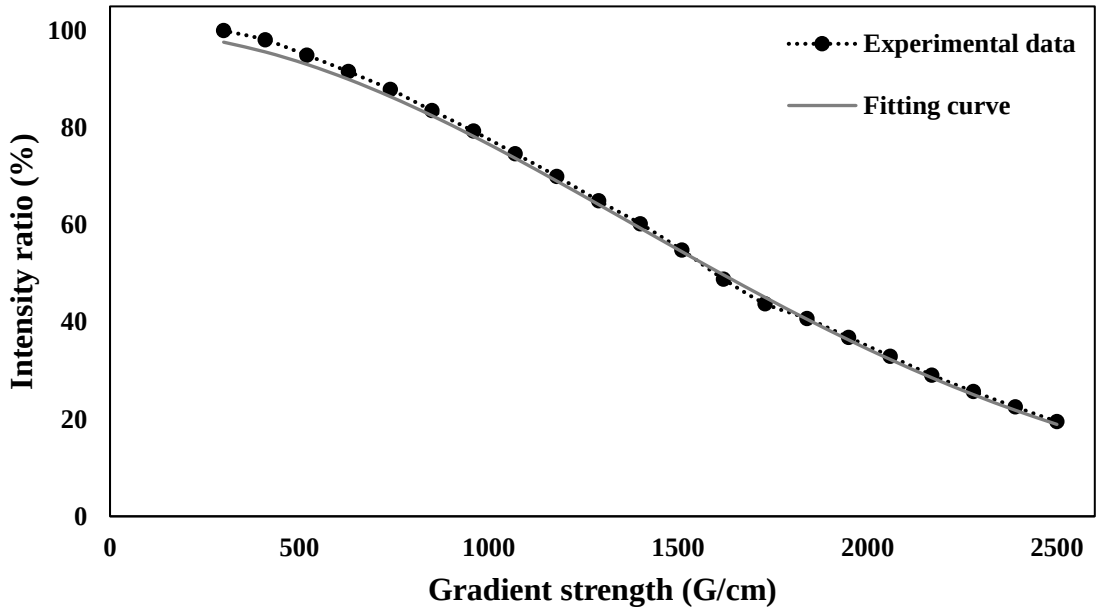

Figure S44. Fitting of **3**-^{t}Bu PFGSE data.

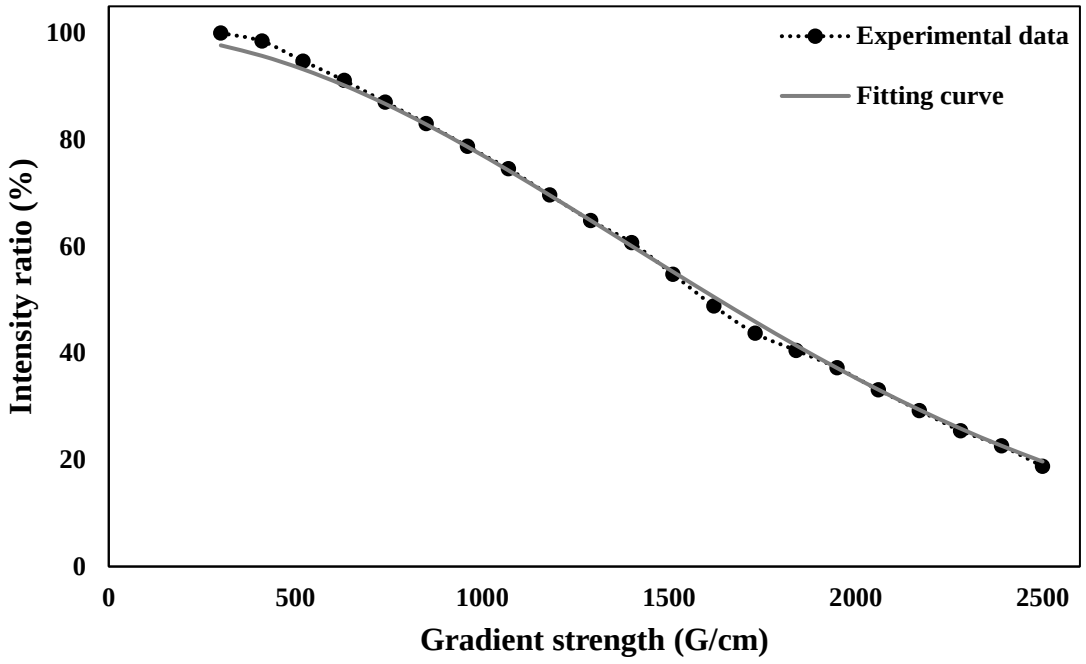

Figure S45. Fitting of **3**-H_a PFGSE data.

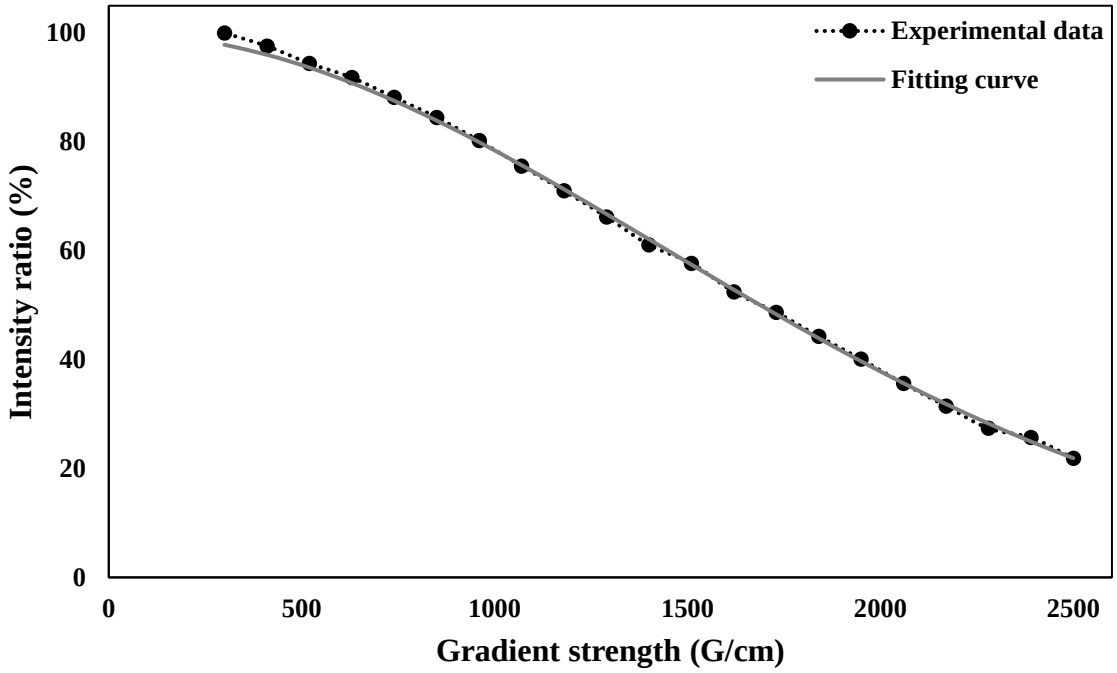

Figure S46. Fitting of $\mathbf{2}_2\cdot\mathbf{3}$-(^{t}Bu) PFGSE data.

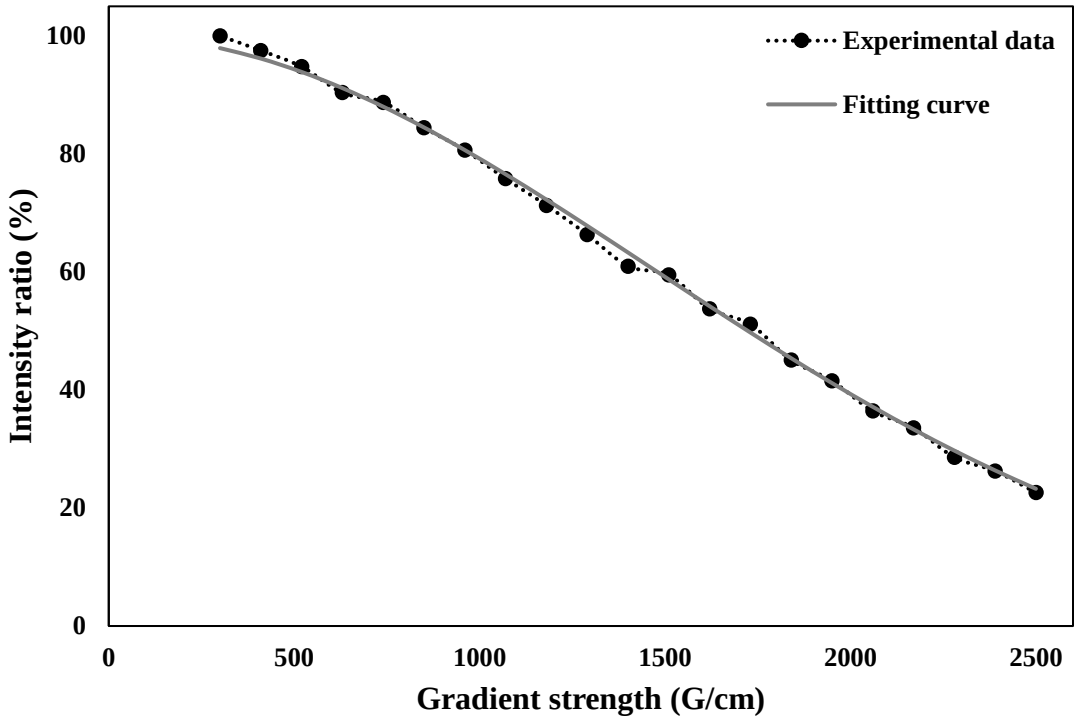

Figure S47. Fitting of $\mathbf{2}_2\cdot\mathbf{3}$-(Me) PFGSE data.

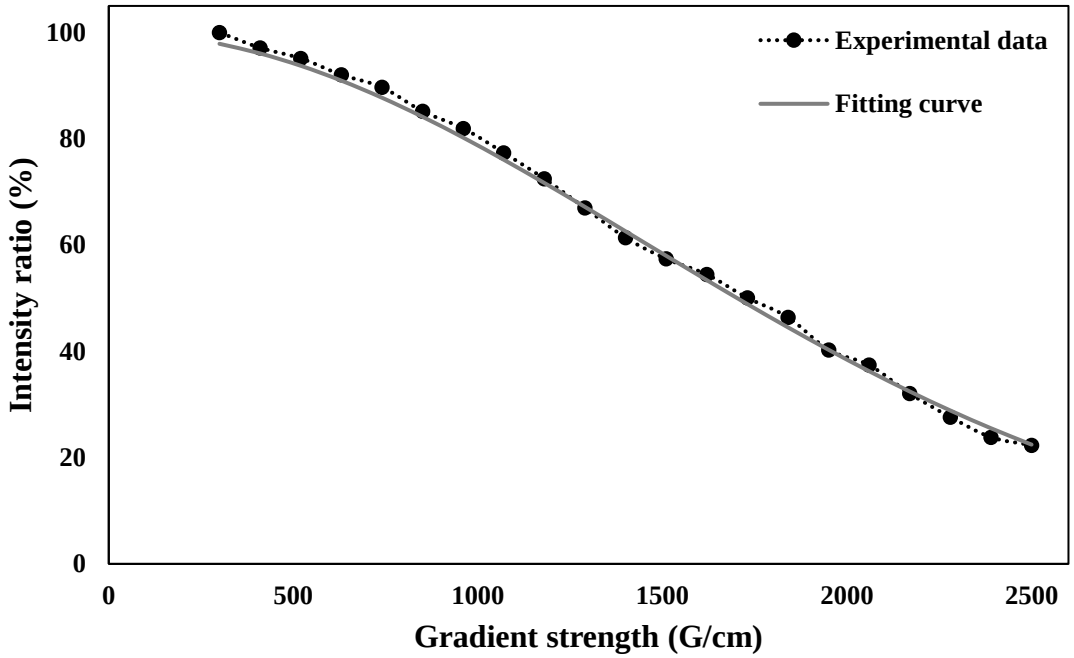

Figure S48. Fitting of $\mathbf{2}_2\cdot\mathbf{3}$-($H_a$) PFGSE data.

S4 References

(1) Zhiquan, L.; Polen, S.; Hadad, C. M.; RajanBabu, T. V.; Badjić, J. D. Russian Nesting Doll Complexes of Molecular Baskets and Zinc Containing TPA Ligands. *J. Am. Chem. Soc.* **2016**, *138* (26), 8253–8258. https://doi.org/10.1021/jacs.6b04436.

(2) Bedard, T. C.; Moore, J. S. Design and Synthesis of Molecular Turnstiles. *J. Am. Chem. Soc.* **1995**, *117* (43), 10662–10671. https://doi.org/10.1021/ja00148a008.

(3) Kiennemann, A.; Levy, G.; Schué, F.; Taniélian, C. Sur La Preéparation de Quelques Tris(Dialycoylamino)-Stibines et Sur Quelques Unes de Leurs Propriétés. *J. Organomet. Chem.* **1972**, *35* (1), 143–148. https://doi.org/10.1016/S0022-328X(00)86892-8.

(4) von, D. H.; Prietzel, H. Weitere Beobachtungen Zur Reaktion Zwischen Aldehyden Und Indolderivaten (III. Mitteil. Zur Chemie Des Indols). *Hoppe-Seyler´s Z. Für Physiol. Chem.* **1955**, *299* (1), 214–226. https://doi.org/10.1515/bchm2.1955.299.1.214.

(5) *APEX3 Data Collection Software, Version 2016.5-0; Bruker AXS: Delft, The Netherlands, 2016*.

(6) Sheldrick, G. i. SADABS, Program for Empirical Absorption Correction of Area Detector Data. *Univ. Gött. Ger.* **1996**.

(7) Sheldrick, G. M. Crystal Structure Refinement with SHELXL. *Acta Crystallogr. Sect. C Struct. Chem.* **2015**, *71* (1), 3–8. https://doi.org/10.1107/S2053229614024218.

(8) Neese, F. *ORCA – an Ab Initio, Density Functional and Semiempirical Program Package, Version 2.9.0*; Max-Planck-Insitut für Bioanorganische Chemie, Mülheim and der Ruhr, 2013.

(9) van Lenthe, E.; Baerends Evert, J.; Snijders, J. G. No Title. *J Chem Phys* **1993**, *99*, 4597–4610.

(10) Heully, J. L.; Lindgren, I.; Lindroth, E.; Lundqvist, S.; Maartensson-Pendrill, A. M. No Title. *J Phys B Mol Phys* **1986**, *19*, 2799–2815.

(11) Grimme, S.; Ehrlich, S.; Goerigk, L. Effect of the Damping Function in Dispersion Corrected Density Functional Theory. *J. Comput. Chem.* **2011**, *32* (7), 1456–1465. https://doi.org/10.1002/jcc.21759.

(12) Weigend, F.; Ahlrichs, R. Balanced Basis Sets of Split Valence, Triple Zeta Valence and Quadruple Zeta Valence Quality for H to Rn: Design and Assessment of Accuracy. *Phys. Chem. Chem. Phys.* **2005**, *7* (18), 3297–3305. https://doi.org/10.1039/B508541A.

(13) Schafer, A.; Horn, H.; Ahlrichs, R. Fully Optimized Contracted Gaussian Basis Sets for Atoms Li to Kr. *J. Chem. Phys.* **1992**, *97* (4), 2571–2577. https://doi.org/10.1063/1.463096.

(14) Weigend, F. Accurate Coulomb-Fitting Basis Sets for H to Rn. *Phys. Chem. Chem. Phys.* **2006**, *8* (9), 1057–1065. https://doi.org/10.1039/B515623H.

(15) Kohn, W.; Sham, L. J. Self-Consistent Equations Including Exchange and Correlation Effects. *Phys. Rev.* **1965**, *140* (4A), A1133–A1138. https://doi.org/10.1103/PhysRev.140.A1133.

(16) Kendall, R. A.; Früchtl, H. A. The Impact of the Resolution of the Identity Approximate Integral Method on Modern Ab Initio Algorithm Development. *Theor. Chem. Acc.* **1997**, *97* (1), 158–163. https://doi.org/10.1007/s002140050249.

(17) Boys, S. F.; Bernardi, F. The Calculation of Small Molecular Interactions by the Differences of Separate Total Energies. Some Procedures with Reduced Errors. *Mol. Phys.* **1970**, *19* (4), 553–566. https://doi.org/10.1080/00268977000101561.

(18) Lu, T.; Chen, F. Multiwfn: A Multifunctional Wavefunction Analyzer. *J. Comput. Chem.* **2012**, *33* (5), 580–592. https://doi.org/10.1002/jcc.22885.
(19) Lu, T.; Chen, F. Quantitative Analysis of Molecular Surface Based on Improved Marching Tetrahedra Algorithm. *J. Mol. Graph. Model.* **2012**, *38*, 314–323. https://doi.org/10.1016/j.jmgm.2012.07.004.
(20) Allouche, A.-R. Gabedit—A Graphical User Interface for Computational Chemistry Softwares. *J. Comput. Chem.* **2011**, *32* (1), 174–182. https://doi.org/10.1002/jcc.21600.
(21) Loya, J. D.; Qiu, J.; Unruh, D. K.; Cozzolino, A. F.; Hutchins, K. M. Co-Crystallization of the Anti-Cholesterol Drug Bezafibrate: Molecular Recognition of a Pharmaceutical Contaminant in the Solid State and Solution via Hydrogen Bonding. *Cryst. Growth Des.* **2018**, *18* (9), 4838–4843. https://doi.org/10.1021/acs.cgd.8b00812.